Dynamic transfer of chirality in photoresponsive systems

Pizzolato, Stefano Fabrizio

Chapter 2

Spectroscopic and Theoretical Identification of Two Thermal Isomerization Pathways for Bistable Chiral Overcrowded Alkenes

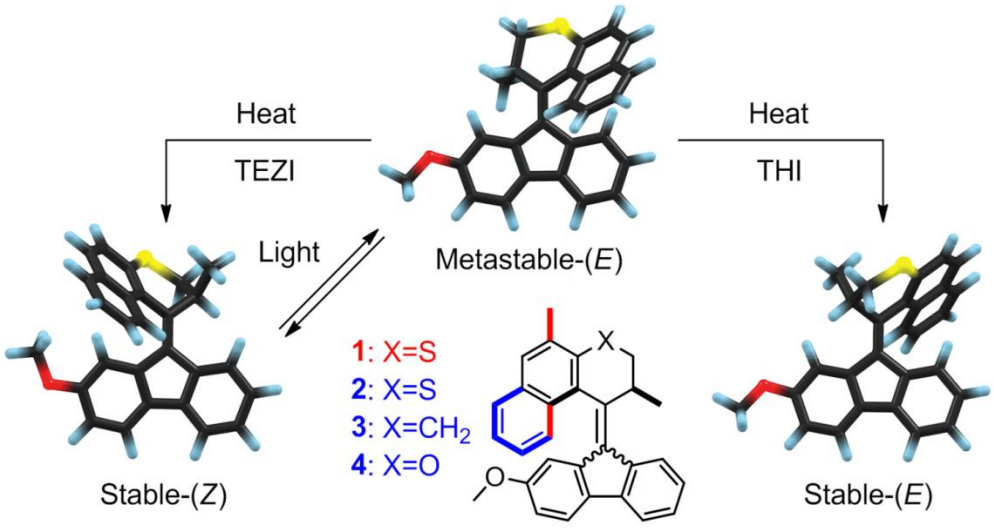

*This chapter presents the synthesis of four chiral overcrowded alkenes **1-4** and the experimental and computational study of their photochemical and thermal behavior . By irradiation with UV light, metastable diastereoisomers with opposite helicity were generated through high yielding E-Z isomerizations. Kinetic studies on the metastable isomers using CD spectroscopy and HPLC analysis revealed two pathways at higher temperatures for the thermal isomerization, namely a thermal E-Z isomerization (TEZI) and a thermal helix inversion (THI). In order to demonstrate that these overcrowded alkenes can be employed as bistable switches, photochromic cycling was performed, which showed that these molecular switches display good selectivity and fatigue resistance over multiple irradiation cycles. The alkenes studied hereto showed a remarkable and unprecedented combination of switching properties including dynamic helicity, reversibility, selectivity, fatigue resistance and thermal stability.*

This chapter has been published as part of: S. F. Pizzolato,[‡] J. C. M. Kistemaker,[‡] T. van Leeuwen, Dr. T. C. Pijper, Prof. Dr. B. L. Feringa,* *Chem. Eur. J.* **2016**, *23*, 13478–13487. [‡] Equally contributing authors.
The computational studies here reported were performed by J. C. M. K. and T. C. P. For more details, see also: J. C. M. Kistemaker, PhD thesis, University of Groningen.

2.1 Introduction

2.1.1 Photo- and thermally-responsive molecular switches

Responsive materials[1–3] and dynamic molecular systems[4–10] that change structure and functions as a result of an external input signal are attracting major current attention with the prospect of smart materials[11–17] and nanoscale devices.[18–22] Photochemical switches allow for non-invasive control, reversibility and high spatio-temporal precision.[5] Overcrowded alkenes have been used in a wide variety of responsive nanoscale systems, being it in a molecular car powered by four unidirectional molecular motors or as multi-state switches featuring dynamic functions of which up to four distinct configurations can be addressed.[23–25] The large number of structural modifications that has been presented by our group and others has expanded the field of molecular design with three generations of photoswitchable overcrowded alkenes, the majority of which exhibits a strong directional preference and functions as rotary motors.[7,26–32] Through desymmetrization of our systems, the unidirectionality of the rotary motion has been extensively demonstrated and various stereoisomers identified by spectroscopic and chromatographic techniques for each variation in design.[33–44] A key aspect of these systems is that the photochemical generation of metastable species is followed by thermally induced isomerizations, for which the life-times have been tuned through structural changes to range from nanoseconds to years.[34,38,44,45] Hence, overcrowded alkenes can be defined as either motors or switches depending on the activation energy and therefore speed of the thermal isomerization step (i.e. when the rotation rate is the limiting step). Their propensity to undergo continuous light- and thermal-induced directional rotary motion (motor behavior), however, diminishes their usefulness as switches in applications where thermal stability is desired, e.g. in the field of photoswitchable catalysis.[24,46,47] As such, there is a demand for thermally highly stable alkenes that can be switched photochemically and reversibly between distinct geometrical chiral forms.

2.1.2 Second generation molecular motors

Molecular motors of the second generation consist of a symmetric 'lower' half (for R=H) and an asymmetric 'upper' half that feature a single stereocenter (Scheme 2.1).[30,48]

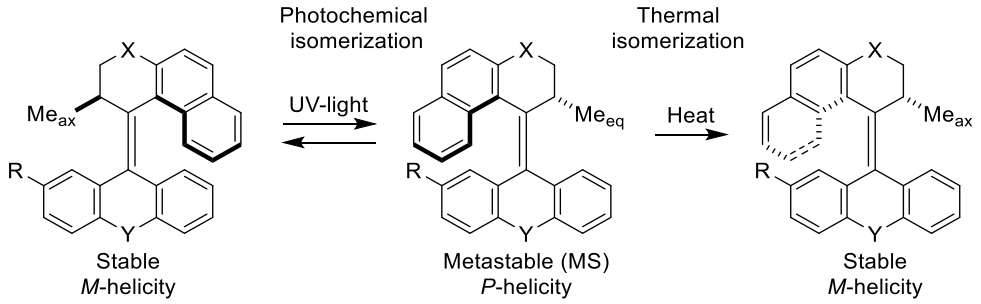

Scheme 2.1. General scheme of photochemical *E-Z* isomerization and thermal helix inversion of second generation molecular motors.

Upon irradiation with UV light they can undergo a photochemical *E-Z* isomerization, a process that results in a metastable (MS) diastereoisomer which is of the opposite helicity. In this process, the methyl substituent on the stereogenic center has changed from an unhindered outward facing axial orientation to an equatorial orientation in which the methyl faces the lower half, thus creating steric hindrance. This steric strain causes the MS diastereoisomer to be higher in energy with respect to the original configuration. The strain can subsequently be reduced by a thermally activated isomerization in which (usually) the upper half moves around the lower half, again resulting in an inversion of the helicity. In the resulting stable isomer, the upper half has undergone a 180° rotation with respect to the lower half (see Scheme 2.1, in case R = H, the symmetry in the lower half causes the initial and final states to be chemically identical). In theory, it is possible that the thermal isomerization of the metastable state follows an alternative and competing

pathway other than thermal helix inversion (THI). Structurally similar stilbene switches are able to undergo thermal *E*-*Z* isomerization (TEZI) from *cis* to *trans*, although the activation energy for this process usually exceeds 150 kJ·mol^{-1}.[49,50] For some overcrowded alkenes though, this barrier has been observed to be significantly lower due to the steric strain in the minimum energy configurations, thus forcing the double bond far from planarity. As an example, bis-fluorenylidenes exhibit activation energies for the TEZI of ~105 kJ·mol^{-1}.[51,52] For second generation motors, in order to positively identify the outcome of the thermal isomerization of the photochemically generated metastable state the lower half has to be desymmetrized. The two-step process starting from the stable-(*Z*) state will then lead either to the opposite isomer stable-(*E*) of the initial configuration, which is indicative of a THI, or back to the initial stable isomer stable-(*Z*), thus indicating a reversible switching process by a TEZI (Scheme 2.2).

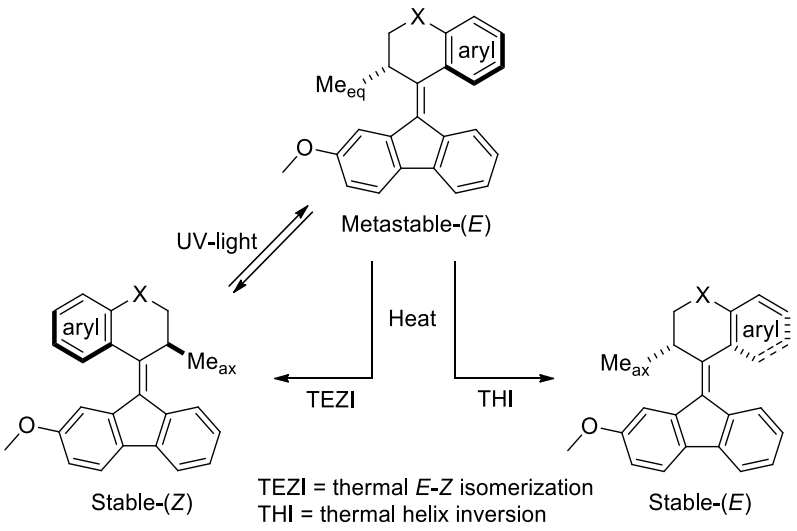

Scheme 2.2. General scheme for photochemical and thermal behavior (TEZI vs. THI) of desymmetrized overcrowded alkenes stable-(*Z*) and metastable-(*E*).

Herein, we report on the switching behavior of four second-generation overcrowded alkenes, namely **1**–**4** (Scheme 2.3). Their photochemical and thermal isomerization processes have been studied by various analytical methods, while the thermal isomerization processes are also studied by computational methods. We will show that the MS isomers of **1**–**4** are able to undergo thermal isomerization through both the THI and TEZI pathways. Finally, we will demonstrate that **1**–**4** exhibit properties that make them highly useful bistable switches, such as high selectivity, low switching fatigue, and high thermal stability.

2.2 Results and discussion

2.2.1 Design

As mentioned above, the bridging units (X and Y, see Scheme 2.1) included in the rings connected by the tetrasubstituted alkene play an important role in the structure's flexibility, thermal stability and switching properties. Previous studies on overcrowded alkenes with symmetrical lower halves have shown the effect of the size of the rings connected to the bridging alkene bond on the activation barrier of the thermal relaxation step.[48] In particular, the combination of a 5-membered ring in the lower half (fluorene) with a sulfur or oxygen containing 6-membered ring in the upper half (Scheme 2.1, benzo[*f*]thiochromene (X=S, Y=–) and benzo[*f*]chromene (X=O, Y=–), respectively) resulted in distinctive high energy activation barriers for the thermal relaxation step and consequently long half-lives of the metastable species ($\Delta^{\ddagger}G°$ = 109 kJ·mol^{-1}, $t_{½}$ at rt = 35 d (X=S) and $\Delta^{\ddagger}G°$ = 106 kJ·mol^{-1}, $t_{½}$ at rt = 9.4 d (X=O), respectively). Due to the lack of asymmetry in the lower half, the two aforementioned competing thermal pathways, i.e. THI and

TEZI, could not be distinguished, as they would give access to the two undistinguishable products. Therefore, we decided to extend our investigation by synthesizing four overcrowded alkenes of the second generation with an asymmetric substitution pattern in the lower half (**1**–**4**, see Scheme 2.3), expecting these systems to display thermal bi-stability.

2.2.2 Synthesis

Overcrowded alkenes **1**-**4** were synthesized according to the established methodology previously reported for second generation molecular motors. The Barton-Kellogg coupling represents a critical synthetic step (Scheme 2.3), in which a combination of highly reactive diazo species and thioketones are joined to create a highly hindered tetrasubstituted alkene moiety through a cascade of exothermic reactions.

Hydrazone **8** was synthesized from commercially available 2,5-dimethylbenzenethiol in four steps with a 54% overall yield (Scheme 2.5). Compounds **9**–**11** with a naphthyl moiety were prepared following modified literature procedures (Scheme 2.3).[58,59] A distinct synthetic scheme for each overcrowded alkene is reported (Schemes 2.5-2.8). A Barton-Kellogg coupling of thioketone **12** (Scheme 2.4) and the diazo species, obtained by the *in situ* oxidation of the corresponding hydrazones **8**–**10** with [bis(trifluoroacetoxy)iodo]-benzene (BTI), afforded mixtures of isomers of episulfides with varying *E*/*Z* ratios. The mixtures were separated by flash column chromatography and subsequently desulfurized in order to obtain the corresponding overcrowded alkenes. A Barton-Kellogg coupling of the diazo species **13** (Scheme 2.4) and the thioketone, obtained by thiation of the corresponding ketone **11**, provided a mixture of alkenes and episulfides which were directly desulfurized, yielding the desired overcrowded alkenes. The *E*/*Z* isomers were separated by column chromatography and assigned by the difference in chemical shift of the absorptions corresponding to the methoxy substituent and the protons in position 1 or 8 at the lower half in the ^{1}H NMR spectra (for example: stable-(*Z*)-**1** 3.42 ppm (CH_3O-), stable-(*E*)-**1** 3.93 ppm (CH_3O-); for full details see Experimental section "Characterization, irradiation experiments and Eyring analysis"). The enantiomers of **1**–**4** were separated by preparative chiral HPLC (Figure 2.2.1, Figure 2.2 and Experimental section for full details).

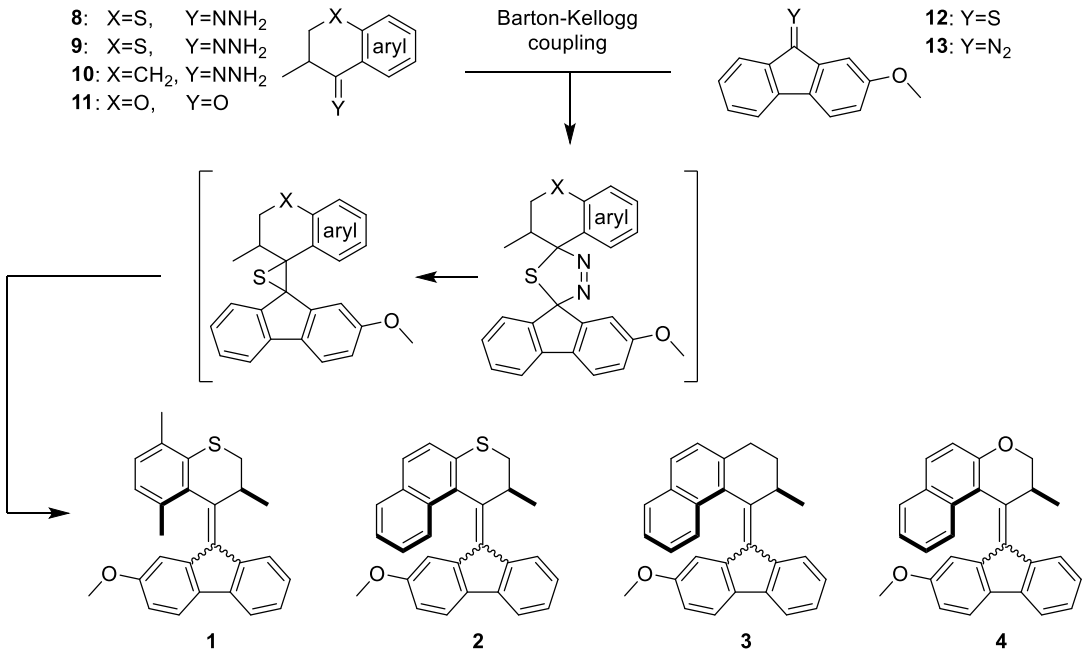

Scheme 2.3. Condensed synthetic pathways towards overcrowded alkenes **1**-**4** via Barton-Kellogg coupling as critical synthetic step.

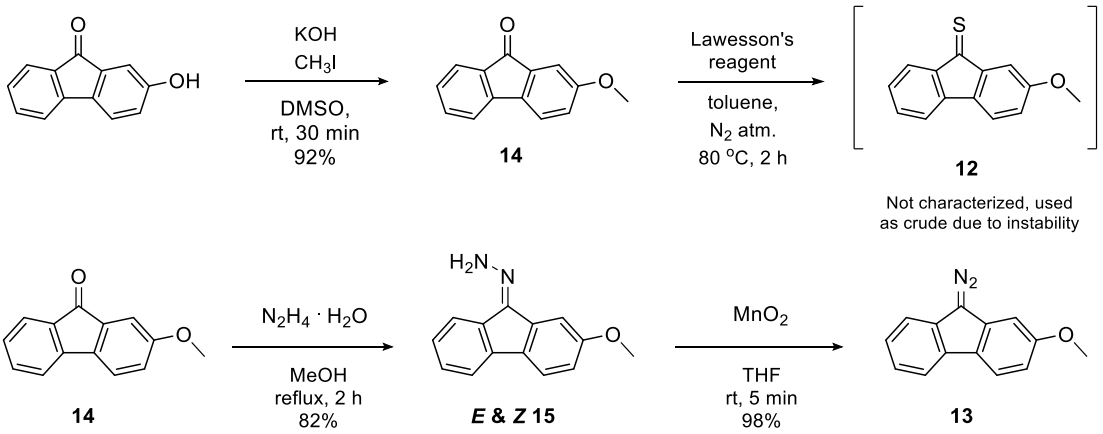

Scheme 2.4. Synthesis of lower halves **12** and **13**.

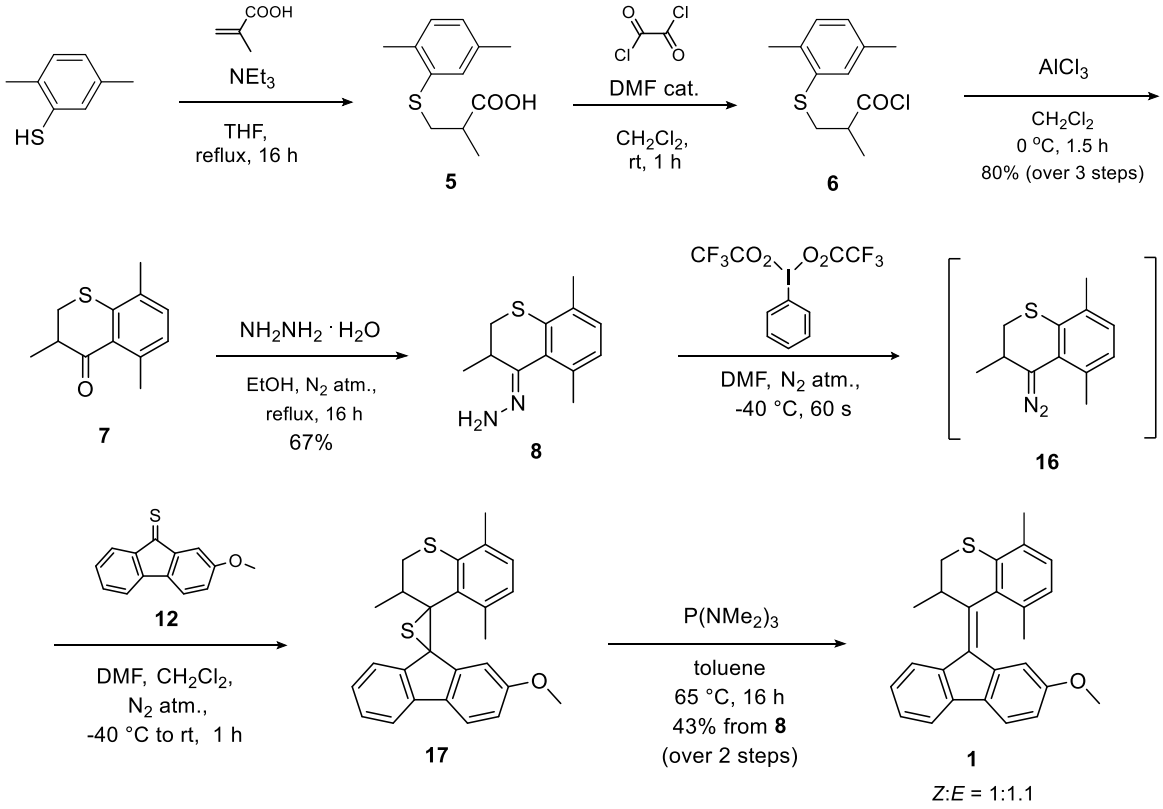

Scheme 2.5. Synthesis of molecular switch **1**.

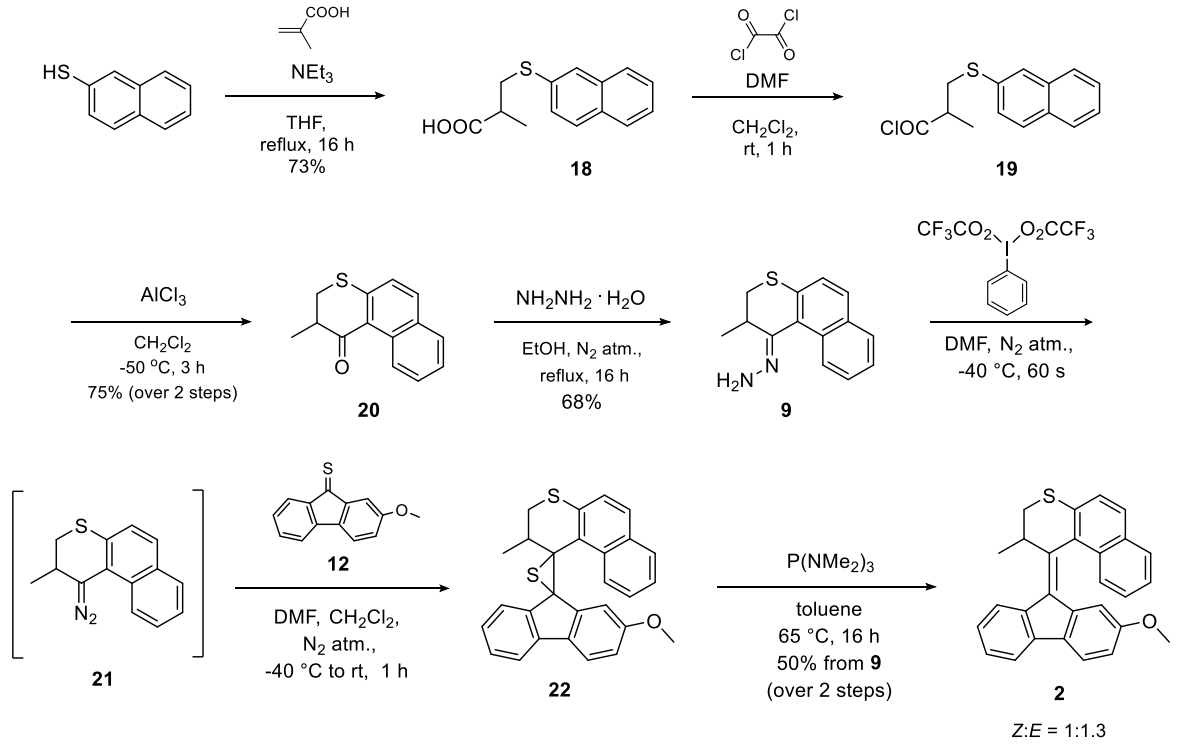

Scheme 2.6. Synthesis of molecular switch **2**.

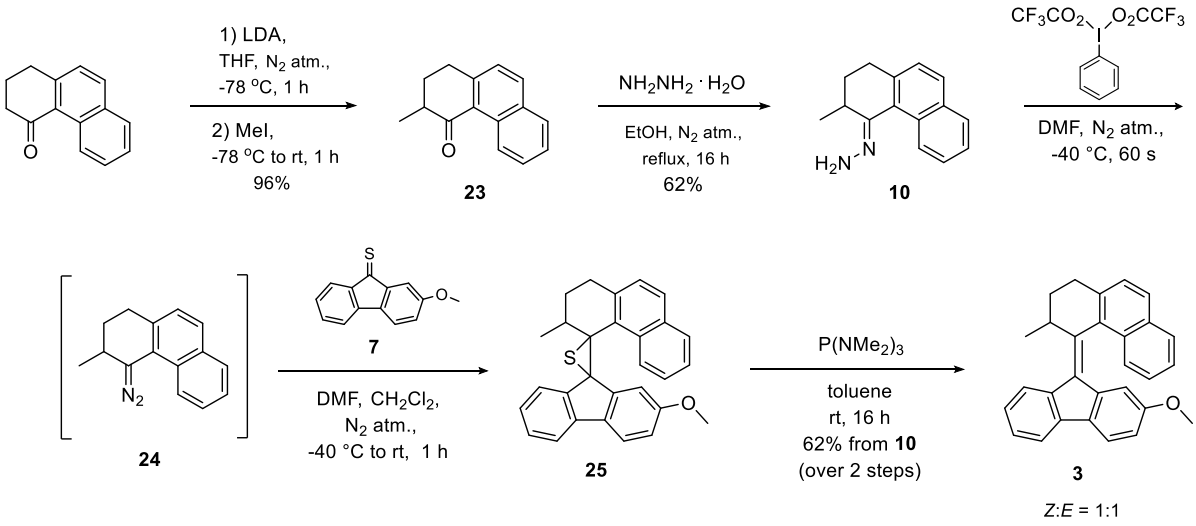

Scheme 2.7. Synthesis of molecular switch **3**.

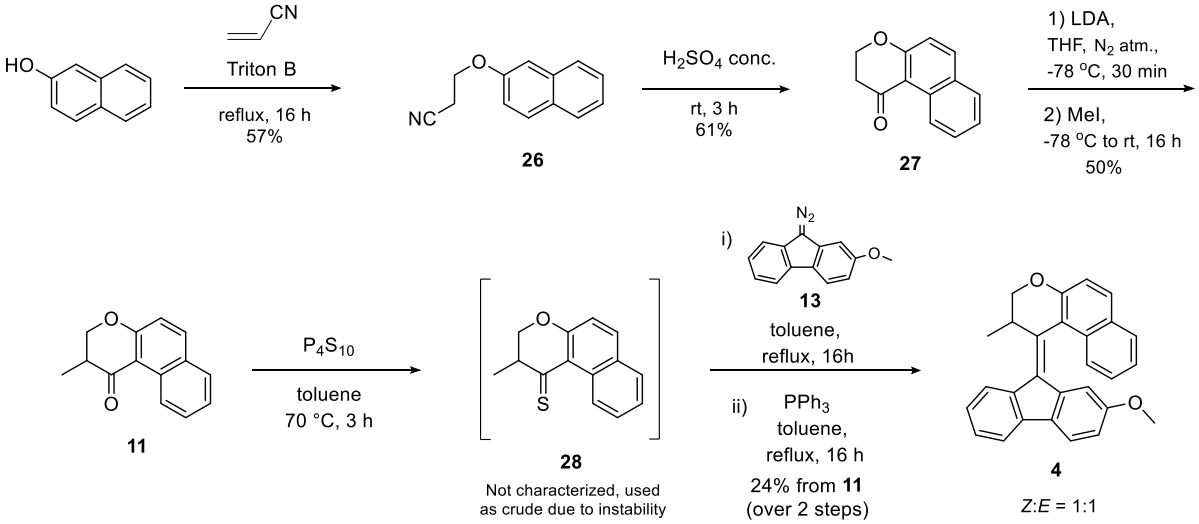

Scheme 2.8. Synthesis of molecular switch **4**, performed by T. van Leeuwen.

2.2.3 Photochemical and thermal isomerizations

Single enantiomers of each overcrowded alkene were subjected to circular dichroism (CD) spectroscopy in order to assign absolute stereochemistry as well as to perform a qualitative analysis. The isolated enantiomers of compounds **1**–**4** displayed strong Cotton effects in the area of ~250–320 nm and slightly smaller Cotton effects of opposite sign at higher wavelengths (>320 nm) with the exception of compound **3** which lacked such a longer wavelength absorption band (Figure 2.1). The presence of such strong Cotton effects around 400 nm is indicative of the helical shape of these overcrowded alkenes, while the lack of this band for compound **3** could be due to the absence of a heteroatom in its core structure (which is present in the other compounds).

In order to assign absolute stereochemistry, experimentally obtained CD spectra were compared to the calculated CD spectra. Potential energy surfaces of **1**–**4** were investigated with the semi-empirical PM3 method and the geometries of the resulting minima and transition states were refined using DFT (B3LYP/6-31G(d,p) (*vide infra*). Time-dependent (TD) DFT with the B3LYP functional and a 6-31+G(d,p) basis set provided theoretical CD spectra of **1**–**4** and allowed for the assignment of the absolute stereochemistries of **1**–**4** (Figure 2.1). Due to the existence of multiple conformations (e.g. of the methoxy group) and the uncertainty in the calculated Boltzmann distribution used to proportionate the spectra of the individual conformations, the calculated spectra were not expected to display a complete match with the experimental data. However, the match is sufficient to allow for the discrimination between the two possible enantiomers and is therefore suitable for the assignment of the absolute stereochemistry of **1**–**4**.[31,40,55,60]

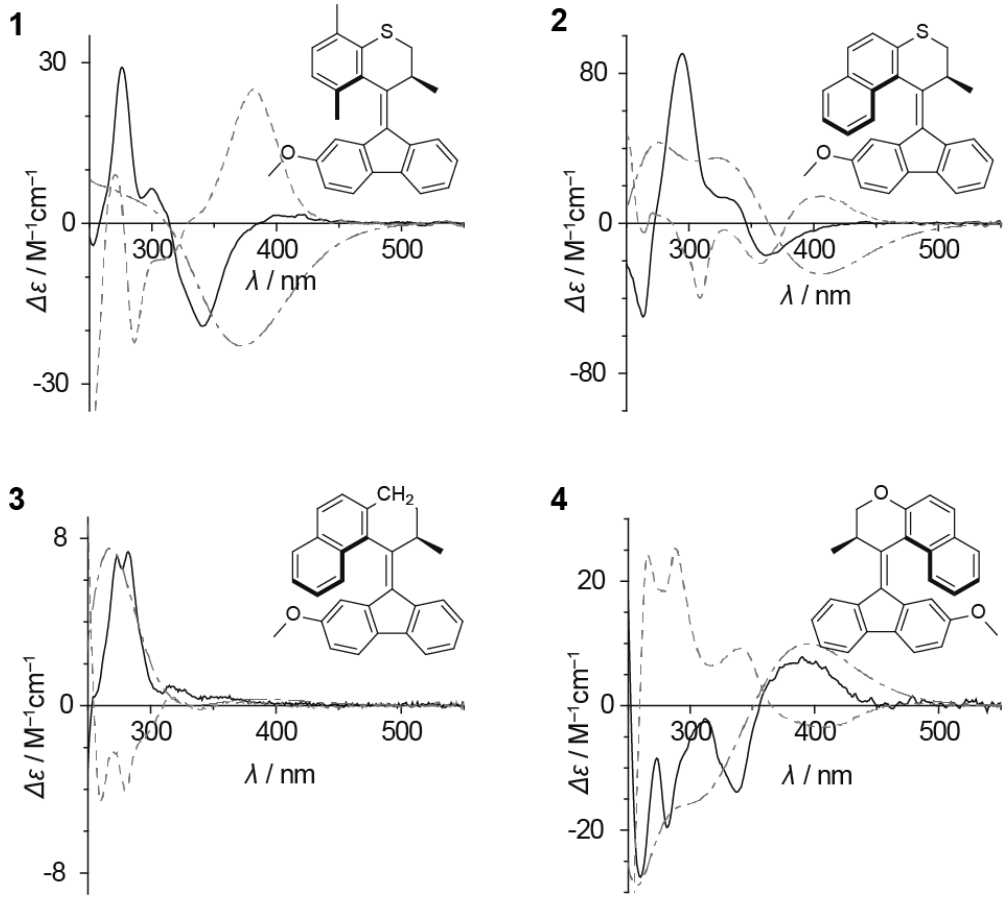

Figure 2.1. CD spectra of **1**–**4.** Solid lines (——): experimental CD spectra of (*Z*,*P*,*S*)-**1**, (*Z*,*P*,*S*)-**2**, (*Z*,*P*,*R*)-**3**, and (*Z*,*M*,*R*)-**4** (heptane, $1.0 \cdot 10^{-5}$ M). Dash and dotted lines (— ▪ —): theoretical ECD spectra calculated with TD-DFT, normalized and shifted by 30 nm (B3LYP/6-31+G(d,p) applying Gaussian shapes (line width = 0.3 eV) to 30 discrete transitions) used to assign enantiomers. Dashed lines (- - -): CD spectra of PSS mixtures of **1** (312 nm), **2** (365 nm), **3** (312 nm), and **4** (365 nm). Irradiation conditions: the PSS mixtures were obtained starting from the above mentioned solutions of stable *Z*-isomers (heptane, $1.0 \cdot 10^{-5}$ M) after irradiation (indicated wavelength) at rt over 2 min.

The chiral descriptors for each species described in this work (e.g. (*Z*,*P*,*S*)-**1**, Figure 2.1) indicate respectively: the configurational isomer of the tetrasubstituted alkene (*E* or *Z*), the configurational helicity of the molecule (*P* or *M*), and the absolute stereochemistry of the stereogenic center (*R* or *S*).
The correlation between the Cotton effect and the helicity agrees with the results of Cnossen et al. in which the same correlation was observed for four different overcrowded alkenes.[55] Compounds with a positive helicity display a negative Cotton effect for the longest wavelength absorption band and vice versa, with the exception of **3** as this species lacks a strong CD absorption band in the 350–450 nm region (*vide supra*).
UV irradiation of solutions in heptane (312 or 365 nm, see Figure 2.1 for details) of each of the *Z* isomers of **1**–**4** resulted in the inversion of the major bands in their CD spectra. This is indicative of an inversion in helicity and shows that the photochemical *Z*-*E* isomerization of the stable-(*Z*)-**1**–**4** to the metastable-(*E*)-**1**–**4** has taken place. The presence of the metastable-(*E*) isomers was further confirmed by chiral HPLC analysis (Figure 2.2) and ^{1}H NMR spectroscopy (illustrated for **1** in Figure 2.3, see Experimental section for further details).

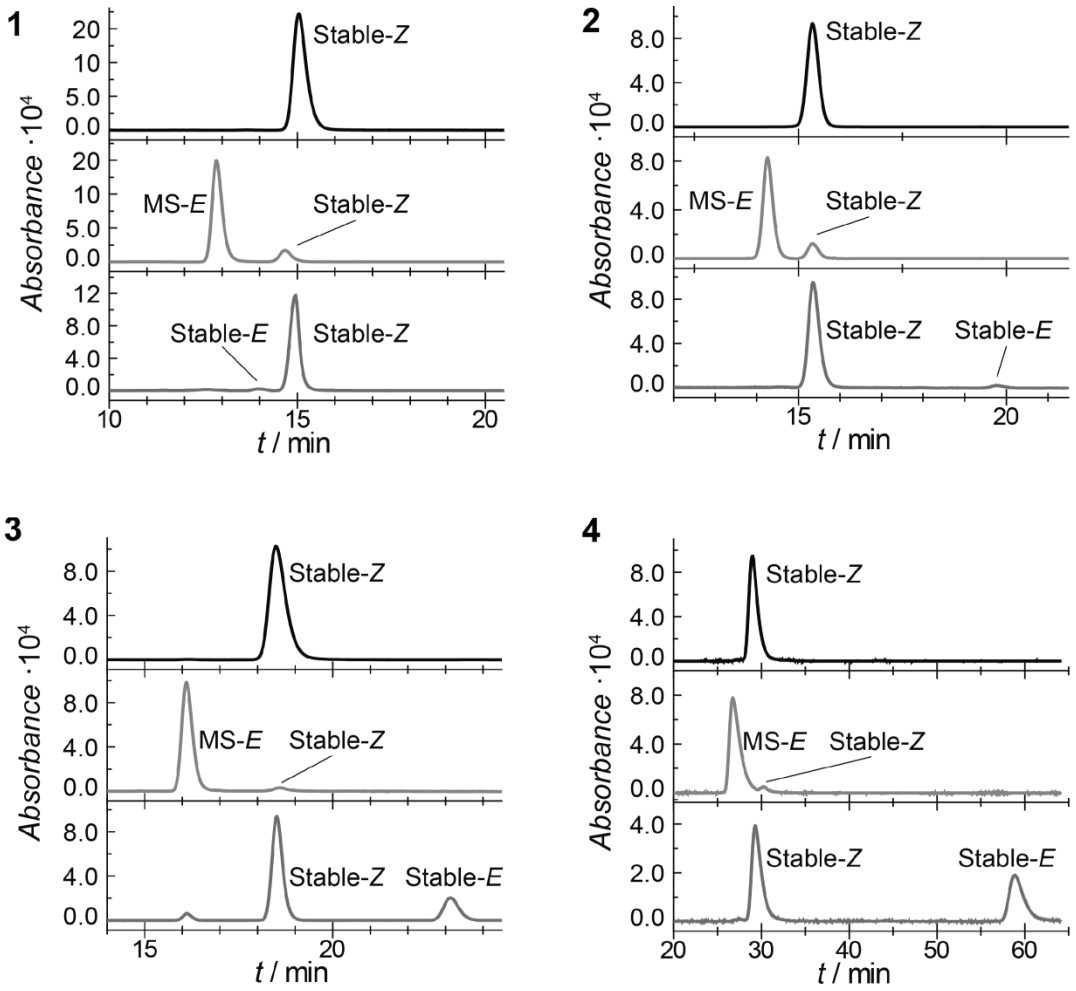

Figure 2.2. Chiral HPLC traces of **1**–**4**. Top: HPLC traces (heptane/2-propanol) of pure enantiomers separated by preparative chiral HPLC (structures of stable-*Z* isomers depicted in Figure 2.1) as assigned by CD absorption spectroscopy: (*Z*,*P*,*S*)-**1** (Chiralcel OD-H, 98:2), (*Z*,*P*,*S*)-**2** (Chiralpak AD-H, 97:3), (*Z*,*P*,*R*)-**3** (Chiralcel OD-H, 98:2), and (*Z*,*M*,*R*)-**4** (Chiralcel OD, 99.3:0.7). Middle: HPLC traces of the PSS mixtures of **1**–**4** (identical conditions). Bottom: HPLC traces after subsequent thermal isomerization of **1**–**4** (identical conditions). For irradiation and thermal isomerization conditions, see Figure 2.1 and Figure 2.4.

The ratio between the *E* and *Z* isomers at the photostationary state (PSS) in heptane solution was determined by chiral HPLC analysis (*E*:*Z* ratio: (*S*)-**1** 95:5, (*S*)-**2** 96:4, (*R*)-**3** 97:3, and (*R*)-**4** 99:1), showing an almost quantitative photoswitching process towards the metastable diastereoisomer for all four compounds, with remarkably high ratios for this class of overcrowded alkene based switches.

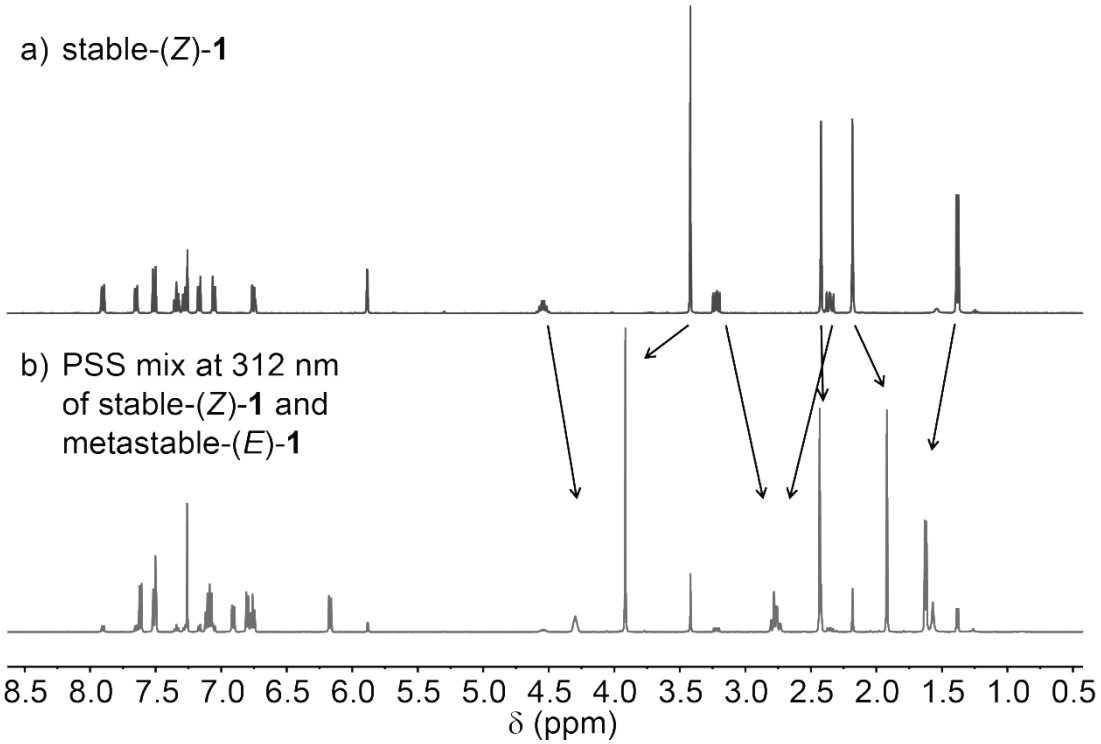

Figure 2.3. ^{1}H NMR spectra of the switching process of **1**. a): ^{1}H NMR spectra of stable-(*Z*)-**1** (~3 mg in $CDCl_3$, 0.8 mL); b): ^{1}H NMR spectra after irradiation of stable-(*Z*)-**1** (312 nm) to the metastable state affording a PSS mixture in $CDCl_3$ of stable-(*Z*)-**1** : metastable-(*E*)-**1** = 16 : 84 (note: PSS ratios are known to be affected by nature of solvent, *vide supra*).

Heating the irradiated samples allowed them to undergo thermal isomerization (for conditions, see Figure 2.4), which resulted in major changes in their CD spectra. HPLC chromatograms of the resulting samples showed a partial reversal of the metastable-(*E*) isomer to the initial, stable-(*Z*) isomer which is observed together with the appearance of a new peak attributed to the stable-(*E*) isomer (Figure 2.2). These results signify: i) that the photochemical *Z* to *E* isomerization results in the formation of a highly stable diastereoisomer that is able to relax measurably only at high temperatures, and ii) that relaxation can take place via two competing pathways, one leading to the initial isomer through TEZI and the other leading to the corresponding *E* isomer through THI (Scheme 2.2).

In order to investigate the kinetic behavior of the two thermal isomerization pathways, samples of alkenes **1**–**4** were irradiated to PSS at room temperature after which their thermal relaxation was followed over time. For alkenes **3** and **4**, thermal relaxation was followed in real-time using CD spectroscopy at the specific wavelength (381 nm and 395 nm, respectively) which showed the largest difference between the initial stable-(*Z*) isomer and the PSS mixture (Figure 2.4). However, for alkenes **1** and **2** this setup was not suitable as the thermal relaxation of these alkenes, in order to become observable, required temperatures that are above the temperature range of the temperature controller of the CD spectrophotometer employed. Instead, solutions of (*Z*,*P*,*S*)-**1** and (*Z*,*P*,*S*)-**2** in hexanol and dodecane, respectively, were irradiated to PSS and placed in a temperature controlled oil bath. Aliquots were then taken regularly and analyzed by chiral HPLC.

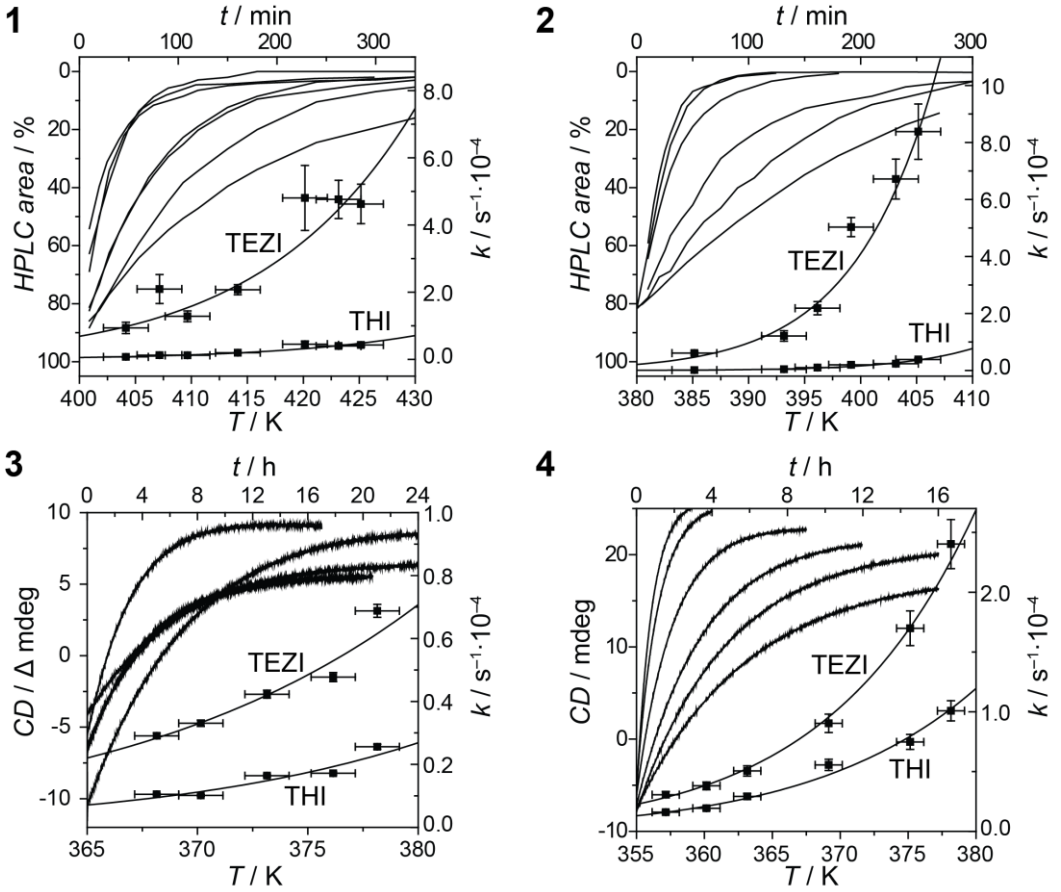

Figure 2.4. Decay curves (top/left axes) and Eyring plots (bottom/right axes) of metastable **1**–**4**. Decay curves of: (*E*,*M*,*S*)-**1** recorded by HPLC taking aliquots from a hexanol solution (131–152 °C); (*E*,*M*,*S*)-**2** recorded by HPLC taking aliquots from a dodecane solution (112–132 °C); (*E*,*M*,*R*)-**3** recorded by CD in dodecane (95–105 °C); (*E*,*P*,*R*)-**4** recorded by CD in dodecane (84–105 °C). Least squares analysis on the original Eyring equation for **1**–**4** with error bars of 3σ. (heptane, $1.0 \cdot 10^{-5}$ M). Thermal decay conditions: the PSS mixtures (hexanol or dodecane, $1.0 \cdot 10^{-5}$ M) were heated at fixed temperatures starting from the above mentioned solutions (black curves) after irradiation with UV light (indicated wavelength) at rt over 2 min under stirring.

A least squares analysis of the HPLC integrals of the major diastereoisomers of **1** and **2** versus time and the change in CD absorption for **3** and **4** versus time provided the reaction rates (k_{total}) for the thermal isomerization process at various temperatures. The thermal isomerization process of these metastable species corresponds to a unimolecular process with two decay paths and a kinetic analysis as a parallel 1st order reactions system can be performed according to what previously described by Forst.[61] The general scheme for two parallel unimolecular reactions is as follows:

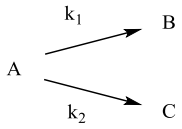

(1)

Starting from a common reagent species A, two distinct product species B and C are obtained with different ratios and rates. The rate law for two parallel unimolecular reactions is described by the following equation:

$$-\frac{d[A]}{dt} = k_{tot}[A] = k_1[A] + k_2[A] \quad (2)$$

The integrated rate law for the decay of the starting species A is described by the following equation:

$$[A] = [A]_0 e^{-(k_1+k_2)t} \quad (3)$$

The integrated rate law for the formation of each product species B and C are described by the corresponding equations as follows:

$$[B] = \frac{k_1[A]_0}{k_1+k_2}\left(1 - e^{-(k_1+k_2)t}\right) \quad (4)$$

$$[C] = \frac{k_2[A]_0}{k_1+k_2}\left(1 - e^{-(k_1+k_2)t}\right) \quad (5)$$

The observed rate constant is the sum of the individual rate constants of formation of B and C (k_1 and k_2):

$$k_{tot} = k_1 + k_2 \quad (6)$$

From the ratio [B]/[C], as it is usually referred to as *branching ratio*, the ratio of rate constants k_1/k_2 can be calculated as follows:

$$\frac{[B]}{[C]} = \frac{k_1}{k_2} \quad (7)$$

Each formation rate constant can then be calculated as follows:

$$k_1 = \frac{k_{tot}}{\left(\frac{[C]}{[B]}+1\right)} \quad (8)$$

$$k_2 = \frac{k_{tot}}{\left(\frac{[B]}{[C]}+1\right)} \quad (9)$$

In this work, A denotes the metastable form, while B and C denotes the two corresponding stable forms:

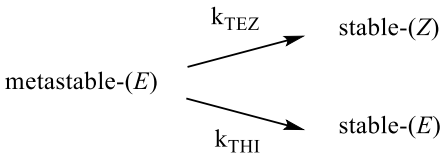

(10)

The observed rate is the sum of the individual rates for TEZI and THI (k_{TEZI} and k_{THI}) and these are related as follows:

$$\frac{k_{\mathrm{TEZI}}}{k_{\mathrm{THI}}} = \frac{[\mathrm{stable}-(Z)]}{[\mathrm{stable}-(E)]} \quad (21)$$

where the final ratio between the stable-(*Z*) and stable-(*E*) isomers is obtained from HPLC after correction for the initial concentration of the stable-(*Z*) isomer at PSS. A least squares analysis of the rates versus the temperature on the original Eyring equation:

$$k = \frac{k_B T}{h} e^{\left(\frac{\Delta^{\ddagger}S^{\circ}}{R}\right)} e^{\left(-\frac{\Delta^{\ddagger}H^{\circ}}{RT}\right)} \quad (13)$$

with appropriate weighing ($1/k^2$) afforded the entropies and enthalpies of activation. The standard errors (σ) were obtained from a Monte Carlo error analysis on the linearized Eyring equation:

$$T \cdot \ln\left(\frac{k}{T}\right) = T \cdot \left(\ln\left(\frac{k_B}{h}\right) + \frac{\Delta^{\ddagger}S^{\circ}}{R}\right) - \frac{\Delta^{\ddagger}H^{\circ}}{R} \quad (14)$$

from forty thousand samples using calculated standard errors on rates and estimated standard errors on temperatures. The kinetic analysis of compounds **1**-**4** was performed according to the general case as described above. In particular for compounds **1** and **2**, in order to calculate the most accurate values, the value of k_{tot} (overall kinetic constant) and σ_{ktot} (standard deviation) at each temperature was obtained, respectively, as average of decay constant of metastable-(*Z*) and formation constant of stable-(*E*) and average of corresponding σ_{st}. The temperature of oil baths during the kinetics experiments was measured with a Pt100 RTD Temperature Sensor and the error ($3\sigma_{st\text{-}T}$) associated, due to the oscillation in temperature over time and between different spots inside the same oil bath, was assumed to be ±2 K. The fitting of formation curves for TEZI and THI processes afforded both the total kinetic constant k_{tot} ($k_{tot} = k_{TEZI} + k_{THI}$) and each extrapolated final value of [st-(*Z*)] and [st-(*E*)] at infinite time. Hence, the branching ratio for each experiment was calculated as the ratio of these two values, from which each k_{TEZI} and k_{THI} could be calculated as described above. For compounds **3** and **4**, a single curve was obtained by monitoring the change of CD signal over time for each fixed temperature. The fitting of the curve afforded the total kinetic constant k_{tot} ($k_{tot} = k_{TEZI} + k_{THI}$) and σ_{ktot} (standard deviation), while the final ratio of [st-(*Z*)] and [st-(*E*)] for each experiment was determined by HPLC analysis. The latter equalled to the branching ratio for each experiment, from which each k_{TEZI} and k_{THI} could be calculated as described above. The temperature of the cuvette during the kinetics experiments was controlled and measured with a Peltier temperature control cell and the error ($3\sigma_{st\text{-}T}$) associated was assumed to be ±1 K. The standard error associated to each kinetic constant was determined through the quadratic variance of each variable. When a function used to calculate a value (*f*) involves multiplications or divisions:

$$f = xy \quad (14)$$

$$f = x/y \quad (15)$$

the associated standard error (σ_f) is calculated from the standard errors of the function parameters (σ_x, σ_y) as follows:

$$\left(\frac{\sigma_f}{f}\right)^2 = \left(\frac{\sigma_x}{x}\right)^2 + \left(\frac{\sigma_y}{y}\right)^2 \quad (16)$$

$$\sigma_f = f\sqrt{\left(\frac{\sigma_x}{x}\right)^2 + \left(\frac{\sigma_y}{y}\right)^2} \quad (17)$$

As described in equations 8 or 9, in this work *f* denotes k_{TEZ} or k_{THI}, while *x* denotes k_{tot} and *y* denotes the branching ratios of TEZ and THI products. The standard error associated to the branching ratios was also determined accordingly. The determination of the error associated with the obtained thermodynamic parameters ($\Delta^{\ddagger}G^{\circ}$, $\Delta^{\ddagger}H^{\circ}$, $\Delta^{\ddagger}S^{\circ}$, $t_{½}$ at rt, T at $t_{½}$=1 h) was performed through Monte Carlo analysis by generation of a large number (40000 hits) of random cases limited in dispersion by the input kinetic constants, temperature and associated standard errors. Eyring analysis for each compound was performed by applying the direct Eyring equation with $1/k^2$ weighing.

$$k = \frac{k_B T}{h} exp\left(-\frac{\Delta^{\ddagger}G}{RT}\right) = \frac{k_B T}{h} exp\left(\frac{\Delta^{\ddagger}S^{\circ}}{R} - \frac{\Delta^{\ddagger}H^{\circ}}{RT}\right) \quad (18)$$

The results of the Eyring analysis are summarized in Table 2.1. From the fitting curves in Figure 2.4 it is evident that the increase in temperature is accompanied by a decrease in accuracy. This is expected for these experiments and therefore an extensive error analysis has been performed to assure the validity of the results from the Eyring analysis. While the error on the derived enthalpy ($\Delta^{\ddagger}H^{\circ}$) and entropy ($\Delta^{\ddagger}S^{\circ}$) of activation are appreciable, the error on the Gibbs free energy of activation ($\Delta^{\ddagger}G$) remains small, particularly

when it is calculated for a temperature in or near the range of temperatures in which the thermal relaxation was observed.

Table 2.1. Kinetic parameters determined by the direct Eyring analysis (Figure 2.4), with standard errors obtained from a Monte Carlo analysis for thermal isomerizations (TEZI and THI) of metastable **1**–**4**.

	(*E*,*M*,*S*)-**1**	(*E*,*M*,*S*)-**2**	(*E*,*M*,*R*)-**3**	(*E*,*P*,*R*)-**4**
$t_{½}$ at rt (years) [a]	75 ±35	4.3±4.2·10^4	1.3 ±0.6	1.3 ±0.2
T at $t_{½}$=1 h (°C)	138.2 ±0.4	121.3 ±0.3	116.0 ±0.7	99.1 ±0.2
$\Delta^{‡}H°_{TEZI}$ (kJ·mol^{-1})	110 ±5.4	184 ±8.1	86.6 ±4.1	108 ±2.6
$\Delta^{‡}S°_{TEZI}$ (J·K^{-1}·mol^{-1})	−51.3 ±13	147 ±21	−98.5 ±11	−30.9 ±7.1
$\Delta^{‡}G°_{TEZI}$ (kJ·mol^{-1}) [b]	129 ±0.6	129 ±0.5	123 ±0.1	120 ±0.5
$\Delta^{‡}H°_{THI}$ (kJ·mol^{-1})	118 ±5.7	208 ±9.2	99.4 ±4.6	96.5 ±2.4
$\Delta^{‡}S°_{THI}$ (J·K^{-1}·mol^{-1})	−53.2 ±14	182 ±23	−72.8 ±12	−68.0 ±6.6
$\Delta^{‡}G°_{THI}$ (kJ·mol^{-1}) [b]	138 ±0.6	140 ±0.6	127 ±0.1	122 ±0.5

[a] rt: 20 °C. [b] Standard condition: 100 °C and atmospheric pressure.

The reason for this is that extrapolation of these parameters to room temperature spans over hundred degrees Celsius for some examples thus magnifying the uncertainty. This is notably observed for the half-life at room temperature, an often reported feature. For example, the standard error determined for the half-life of **2** is as large as the half-life itself. Therefore, we report a more appropriate characteristic of the first order reaction, namely the 'hour half-life temperature' which is the temperature at which the half-life equals one hour. This property is not an extrapolation but usually falls within or close to the range of measured temperatures and is derived from the Eyring equation by the use of the Lambert W function[62] as in the following equation:

$$T_{t_{1/2}=1\mathrm{h}} = \Delta^{‡}H° \cdot \left(R \cdot W\left(\frac{3600 \cdot k_B \cdot \Delta^{‡}H° \cdot e^{\frac{\Delta^{‡}S°}{R}}}{h \cdot R \cdot \ln(2)} \right) \right)^{-1} \qquad (19)$$

The error on the parameters discussed for different processes is reduced to less than a percent of the parameter. Moreover, the temperature at which the half-life equals one hour is a much more chemically intuitive feature, particularly when the half-lives at room temperature of the processes under investigation are over a year or even exceeding forty thousand years (as for (*E*,*M*,*S*)-**2**).

Going from oxygen in **4** (X=O), carbon in **3** (X=C), to sulfur in **2** (X=S), the hour half-life temperature increases from 99 to 116 and 121 °C, indicating an increase in stability of the metastable diastereoisomer. Furthermore, substituting the xylene moiety in **1** for the naphthalene moiety in **2** increases the hour half-life temperature even further to 138 °C. From the Gibbs free energy of activation for the two possible pathways it is clear that under standard conditions the TEZI pathway is preferred over the THI pathway. Plotting the Gibbs free energy versus temperature (Figure 2.5), hereby assuming that the enthalpy and entropy are temperature independent, reveals that for the entire temperature range under investigation (experimental temperature range: 85–152 °C) the barrier for the TEZI is lower than that for the THI for all alkenes **1**–**4**.

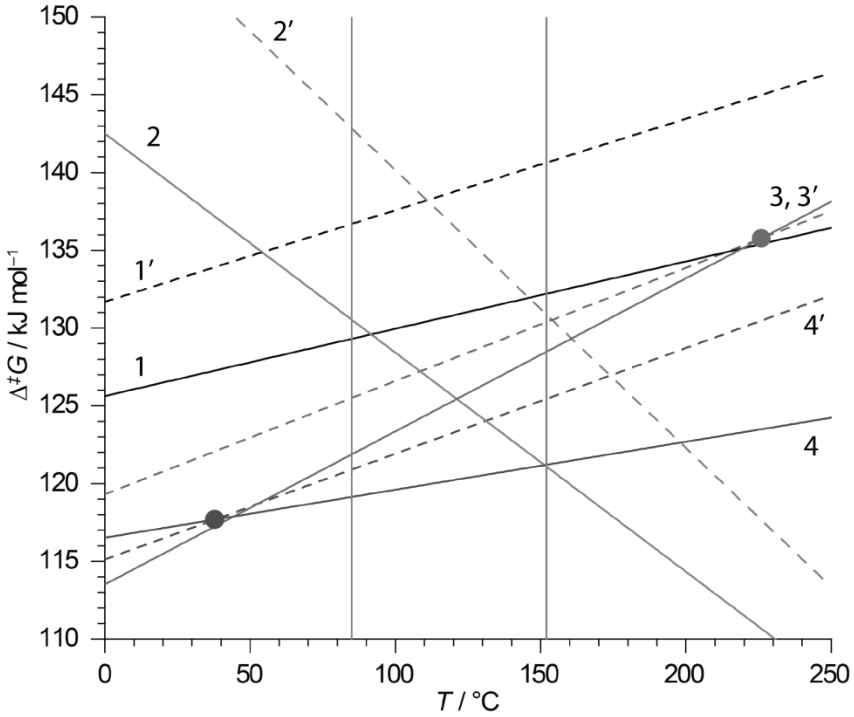

Figure 2.5. Gibbs free energy of activation for the TEZI (solid lines) and the THI (dashed lines) processes plotted vs. temperature for the metastable-(*E*)-diastereoisomers of alkenes **1**–**4**. The experimental temperature range is marked by grey vertical lines (85–152 °C), inversion points for the two processes are marked for **3** and **4** by a dot. Inversion points for **1** and **2** fall outside measurable ranges of temperature and free Gibbs energy.

A difference in the entropy of activation for the two processes logically leads to the existence of a point at which the rates for the two processes are expected to be equal. Such a point would signify the inversion of the two processes, because beyond this temperature the barrier of the THI will be lower than that of the TEZI. For alkenes **3** and **4**, these points are found at relevant temperatures (226 °C and 37.8 °C, respectively) while for **1** and **2** the inversions would take place either far outside of the experimentally significant temperature range or never at all (411 °C and <0 K, respectively).

2.2.4 Computational results

Previously, research on molecular motors has to a large extent been supported by computational chemistry.[31,48,53–55] For example, it has been shown that the energy barrier of the thermal helix inversion can be predicted with reasonable accuracy (within several kJ·mol^{-1}) through the use of density functional theory (DFT) at the B3LYP/6-31G(d,p) level.[31,44,48,53,55] Indeed, this method has been utilized to design new motors *in silico* by prediction of the helix inversion energy barriers of motors prior to their synthesis in order to determine whether their rotation rates would be of the desired order of magnitude. The experimental study of the thermal behavior of the metastable diastereoisomers (*E*)-**1**–**4** was accompanied by a computational study of the potential energy surface of overcrowded alkenes **1**–**4**. As such computational studies were entirely executed by J. C. M. Kistemaker and Dr. T. C. Pijper, the reader should refer to the published version of the current work for a more more detailed discussion of the computational approach used. The results obtained have been reported here for comparison with experimental data.

The calculated Gibbs free energies are summarized for alkenes **1**–**4** in Table 2.2 and the obtained geometries for (*S*)-**2** are depicted in Figure 2.7 as an example. The geometries of **1**, **3** and **4** do not differ significantly in general appearance from those of **2**, although they naturally do differ in specific bond angles and lengths. Going from alkene **4** to alkene **3** to alkene **2**, the size of the bridging atom X in the

upper half increases, which is accompanied by an increase in the size of that ring and thus forces the aryl moiety towards the lower half (Figure 2.6b, Table 2.2). The increase in steric hindrance is alleviated by additional folding of the six-membered ring, as can be seen from the dihedral angle made up by atoms 1, 2 and the central alkene (as indicated in Figure 2.6a for the metastable-(*E*) isomer). Both **1** and **2** are bridged by a sulfur atom and therefore hardly differ in ring size, although the difference between the aryl and xylyl moieties is to a small extent reflected by their dihedral angles (see 'dihedral angle' in Table 2.2). The barrier for the THI increases with an increase in the degree of folding of the upper half, as is seen from the dihedral angle. A similar increase is observed for the calculated barrier for the TEZI, with the exception of **1** which exhibits a significantly higher barrier without an increase in folding with respect to **2**.

Table 2.2. Relative Gibbs free energies of **1**–**4** calculated at the DFT-B3LYP/6-31G(d,p) level or MRMP2/CASSCF(14,14)/6-31G(d) // CASSCF(10,10)/6-31G(d) level indicated by * (373.15 K, 1 atm, in $kJ \cdot mol^{-1}$).

	(*S*)-**1**	(*S*)-**2**	(*R*)-**3**	(*R*)-**4**
Stable-(*Z*)	0	0	0	0
TS TEZI*	165	150	146	138
Metastable-(*E*)	22.2	23.1	27.2	24.9
TS THI	163	165	151	146
Stable-(*E*)	0.94	1.74	1.89	1.46
MS-(*E*) X-ring size (pm)[a]	961	958	901	875
MS-(*E*) dihedral angle (°)[b]	46.7	47.6	42.6	41.4

[a] Summed lengths of the bonds making up the six-membered ring in the upper half (Figure 2.6b).
[b] Dihedral angle made up by atoms 1, 2 and the central alkene as indicated in Figure 2.6a.

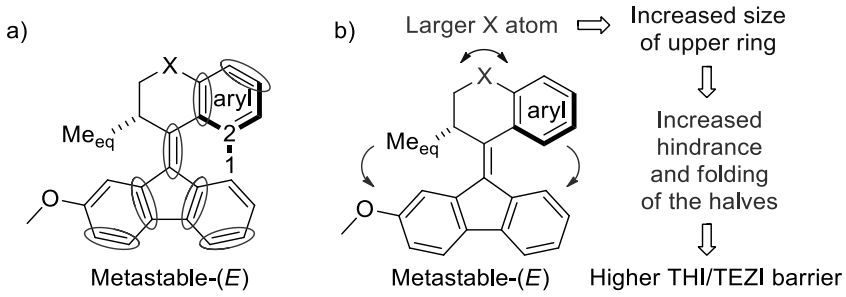

Figure 2.6. a) Active space used in CASSCF(14,14) and MRMP2/CASSCF (14,14) calculations. π bonds included are indicated with circles. b) Correlation between X-ring size and thermal relaxation energy barrier.

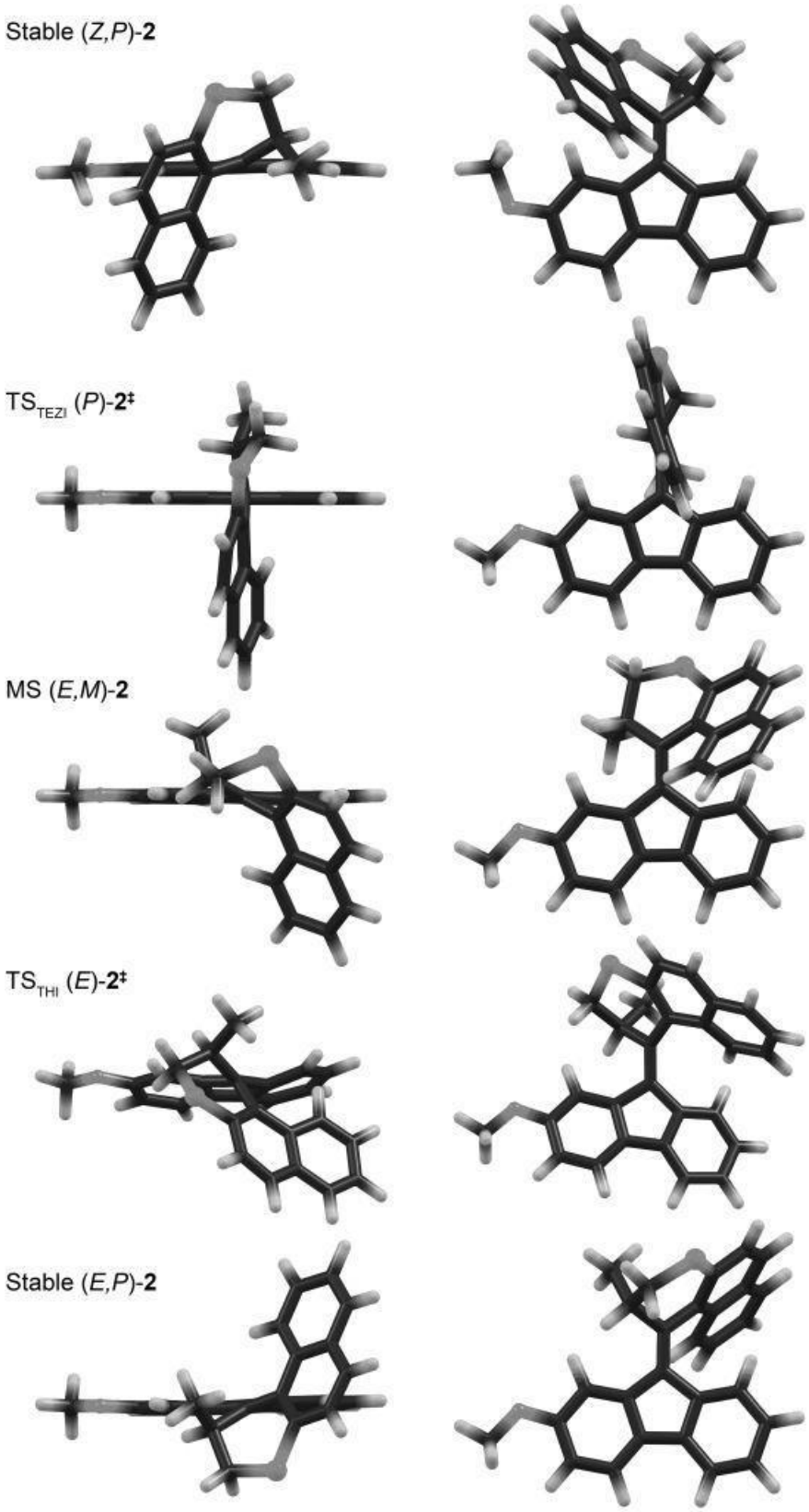

Figure 2.7. Calculated geometries of (*S*)-**2** (X = S). Left: top view with the upper half on top, the alkene on the z-axis and the fluorene in the x-z plane, right: front view with the alkene on the y-axis and the fluorene in the x-y plane. Calculations and rendering performed by J.C.M. Kistemaker.

Table 2.3 provides an overview of the experimentally determined and calculated Gibbs free energies of activation for the TEZI and THI pathways for alkenes **1**–**4**. The calculated barriers for the THI agree strongly with those found experimentally, differing no more than 3 kJ·mol^{-1}. The calculated barriers for the TEZI deviate more from the experimentally determined barriers. The barriers of **2** and **3** correspond well whereas the barrier of **1** is overestimated and the barrier of **4** is slightly underestimated. The slight underestimation of the TEZI barrier for **4** still allows for a reasonable prediction of the behavior of the overcrowded alkene, however, the overestimated barrier of **1** suggests almost equal rates for the THI and TEZI processes while experimental results show the TEZI pathway to be significantly faster than the THI pathway. This could imply that the computational approach used herein may not be as accurate for overcrowded alkenes with xylene-derived upper halves as it is for those with naphthalene-derived upper halves. Nonetheless, these computational methods provide valuable insight how the thermal isomerization behavior relates to the geometric changes in these second generation overcrowded alkenes.

Table 2.3. Comparison of experimental and theoretical barriers for TEZI and THI of **1**–**4**.[a]

Metastable:	(*E*)-**1**	(*E*)-**2**	(*E*)-**3**	(*E*)-**4**
$\Delta^{\ddagger}G°_{TEZI}$ (kJ·mol^{-1})	129±0.6	129±0.5	123±0.1	120±0.5
$\Delta^{\ddagger}G^{calc}_{TEZI}$ (kJ·mol^{-1})	142	127	119	113
$\Delta^{\ddagger}G°_{THI}$ (kJ·mol^{-1})	138±0.6	140±0.6	127±0.1	122±0.5
$\Delta^{\ddagger}G^{calc}_{THI}$ (kJ·mol^{-1})	141	142	124	121

[a] standard condition: 100 °C and atmospheric pressure.

2.2.5 Photoswitching process

It was found that the increased thermal stability of the metastable states of alkenes **1**–**4** makes them very suitable candidates for use as bistable photoisomerisable switches. The switching properties of **1**–**4** (Scheme 2.9) were monitored by UV-vis absorption spectroscopy (Figure 2.8) and ^{1}H NMR spectroscopy (*vide supra*).

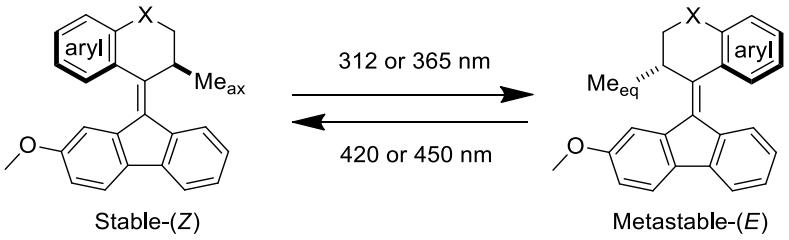

Scheme 2.9. General scheme for reversible highly selective photoswitching of stable (*Z*)-**1**–**4** and metastable (*E*)-**1**–**4**.

Solutions of stable **1**–**4** (heptane) in quartz cuvettes were irradiated at room temperature for a few minutes towards either the metastable state using UV light (312 or 365 nm) or the stable state using visible light (420 or 450 nm). Using UV-vis absorption spectroscopy, the reversible photochemical *E*-*Z* isomerizations were found to be characterized by clear isosbestic points, indicating the absence of side reactions, as well as bathochromic shifts of the major absorptions bands in the metastable state of about 30–80 nm. This is in full agreement with the calculated structural change and concomitant change in the HOMO-LUMO gap. Upon the formation of the metastable state the overcrowded alkene experiences an increase in twist as is illustrated in the calculated structures in Figure 2.7. This twisting increases the energy of the HOMO by an average 23 μeV for **1**–**4** while at the same time lowering the LUMO by an average 246 μeV, which together

significantly reduces the HOMO-LUMO gap. This is opposite to the observations of Cnossen *et al.* for second generation molecular motors with six membered rings in both the upper as well as lower half in which the twist over the double bond was lowered in the metastable state and a hypsochromic shift was observed.[55] The bathochromic shift upon formation of the metastable **1**–**4** allows for a highly selective photochemical switching process in which both states can be addressed by the use of light of an appropriate wavelength (Scheme 2.9, Figure 2.8). None of the overcrowded alkenes showed any noticeable degradation over multiple switching cycles, thus exhibiting an excellent fatigue resistance of this family of molecular switches.

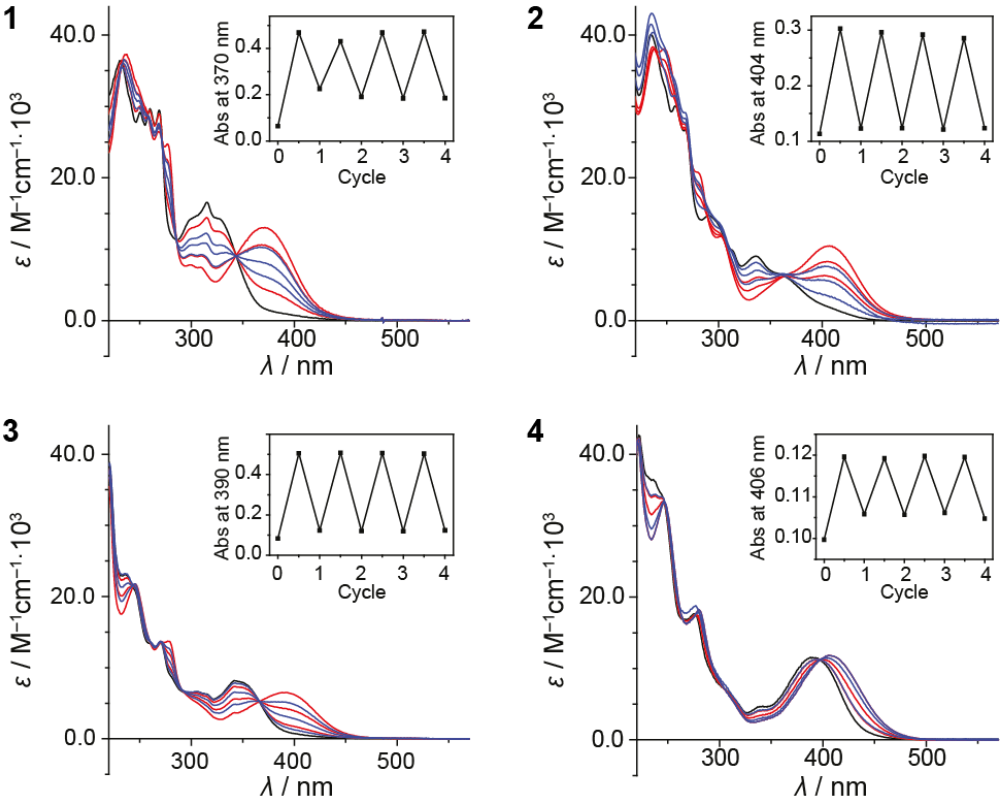

Figure 2.8. UV-vis spectra of the switching process of **1**–**4**. Experimental UV-vis absorption spectra in black of (*Z*,*P*,*S*)-**1**, (*Z*,*P*,*S*)-**2**, (*Z*,*P*,*R*)-**3**, (*Z*,*M*,*R*)-**4** (heptane, $1.0 \cdot 10^{-5}$ M). Irradiation of **1** (312 nm), **2** (365 nm), **3** (312 nm), and **4** (365 nm) to the metastable state affords a PSS shown in red with two intermediate moments in the process shown as well in red (*E*:*Z* ratio: (*S*)-**1** 95:5, (*S*)-**2** 96:4, (*R*)-**3** 97:3, and (*R*)-**4** 99:1). Irradiation using a longer wavelength of **1** (420 nm), **2** (450 nm), **3** (420 nm), and **4** (450 nm) allowed for the reversed *E*-*Z* isomerization towards the stable state affording a new PSS shown in blue with two intermediate moments in the process shown as well in blue (*Z*:*E* ratio; (*S*)-**1** 64:36, (*S*)-**2** 82:18, (*R*)-**3** 97:3, (*R*)-**4** 70:30). Inserts display irradiation cycles between the two PSS's for each compound.

The PSS ratios for the stable-(*Z*) to metastable-(*E*) isomerizations obtained upon irradiation with UV light were determined by HPLC and were all found to yield ≥ 95% of the metastable-(*E*) state for the forward isomerization (*vide supra*). The reverse reaction using visible light afforded varying PSS ratios (*Z*:*E* ratio; (*S*)-**1** 64:36, (*S*)-**2** 82:18, (*R*)-**3** 97:3, (*R*)-**4** 70:30),[63] as determined by HPLC and/or UV-vis (see Experimental section). Alkene **3** hereby displayed the most efficient photoswitching, producing 97% of the opposite diastereoisomer in both directions, and would therefore be the most suitable candidate for use as a bistable photocontrolled switch. With respect to thermal stability, overcrowded alkene **1** exhibits the most favorable behavior , possessing an hour half-life temperature of 138 °C. This is over 22 °C higher than that

of **3** and the TEZI of **1** yields the starting isomer almost exclusively (>94%), making it remarkably bistable as well as selective during the thermal isomerization.

2.2.6 Full experimental study of stable *E*-isomer isomers

The discussion held so far comprises the experimental and computational studies focused for simplicity only on the stable *Z*-isomer isomers of **1**-**4** and the species directly involved via their photochemical and thermal isomerization. A full experimental characterization of the analogous species obtained via isomerization of stable *E*-isomer isomers of **1**-**3** and the thermal relaxation of their photo-generated metastable *Z*-isomer isomers of **1**-**3** (Scheme 2.10) was also performed and is summarized in the current section.

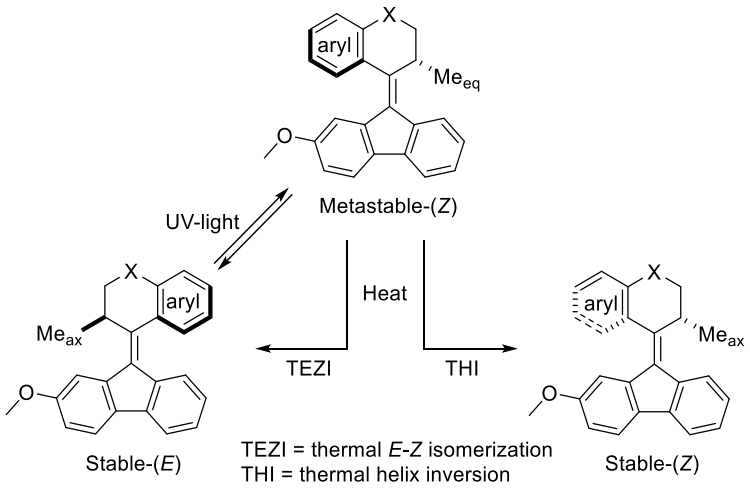

Scheme 2.10. General scheme for photochemical and thermal behavior (TEZI vs. THI) of desymmetrized overcrowded alkenes stable-(*E*) and metastable-(*Z*).

As their properties are strictly related to their main scaffold and influenced to a lower extend by the position of the methoxy-substituent located on the fluorenyl lower half, their photochemical and thermal properties do not differ significantly from their diastereoisomeric counterparts described in the previous sections. It is worth to mention that compound **4** had been synthesized and characterized by J. C. M. Kistemaker and T. van Leeuwen prior to this work and no investigation of the *E*-isomer isomers of **4** was performed at the time.

Similarly, to the Z-isomers (see section 1.2.3), metastable *E*-isomer isomers of **1**-**3** were subjected to photo-chemical isomerization to the corresponding metastable *Z*-isomer upon monitoring via CD and UV-vis abs. spectroscopy. The isolated enantiomers of compounds **1**–**3** displayed strong Cotton effects in the area of ~250–320 nm and slightly smaller Cotton effects of opposite sign at higher wavelengths (>320 nm) with the exception of compound **3** which lacked such a longer wavelength absorption band (Figure 2.9). The presence of such strong Cotton effects around 400 nm is indicative of the helical shape of these overcrowded alkenes, while the lack of this band for compound **3** could be due to the absence of a heteroatom in its core structure (which is present in the other compounds). The assignment of the absolute configuration of each enantiomer was performed by comparison with the calculated and experimental CD spectra of the corresponding stable Z isomers (see Figure 2.1).

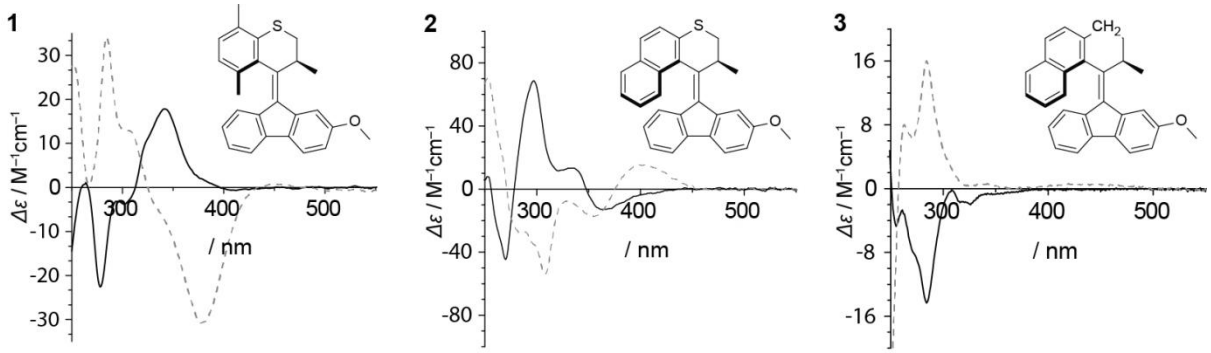

Figure 2.9. CD spectra of (*E*)-**1**–**3**. Experimental CD spectra in solid lines of (*E*,*M*,*R*)-**1**, (*E*,*P*,*S*)-**2**, (*E*,*M*,*R*)-**3** (heptane, $1.0 \cdot 10^{-5}$ M). CD spectra in dashed lines of PSS mixture of **1** (irrad. at 312 nm), **2** (irrad. at 365 nm), **3** (irrad. at 312 nm).

The switching properties of (*E*)-**1**–**3** were monitored by UV-vis absorption spectroscopy. Solutions of stable (*E*)-**1**–**3** in a quartz cuvette were irradiated at rt over a few minutes, forming the metastable forms by irradiation with shorter wavelength light (312 or 365 nm) or the stable forms by irradiation with longer wavelength light (420 or 450 nm) (*vide supra*). For each compound, the reversible photo-induced isomerization process of each compound is characterized by a clear isosbestic point and by a clear redshift of the major absorption band by ~30–80 nm. As reported in the corresponding graphs, the compounds showed no degradation over multiple switching cycles (Figure 2.10).

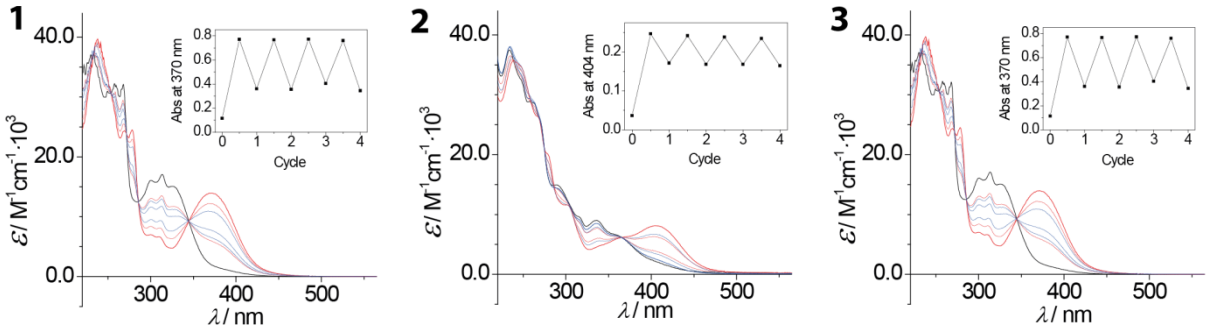

Figure 2.10. UV-vis spectra of the switching process of (*E*)-**1**–**3**. Experimental UV-vis absorption spectra in black of (*E*,*M*,*R*)-**1**, (*E*,*P*,*S*)-**2**, (*E*,*M*,*R*)-**3** (*heptane*, $1.0 \cdot 10^{-5}$ M). UV-vis absorption spectra in red of PSS towards metastable species of (*E*)-**1** (312 nm), (*E*)-**2** (365 nm), (*E*)-**3** (312 nm) with two intermediate moments during irradiation process. UV-vis absorption spectra in blue of PSS towards stable species of (*E*)-**1** (420 nm), (*E*)-**2** (450 nm), (*E*)-**3** (420 nm) with two intermediate moments during reverse irradiation process. Inserts display irradiation cycles between the two PSS's for each compound as monitored by UV-vis absorption at each specific local maximum of the corresponding metastable species.

HPLC analysis of the various solutions afforded the composition of each PSS mixture (irradiation at 312 or 365 nm and 420 or 450 nm, respectively) in heptane, as well as the composition of each PSS mixture after thermal decay (Figure 2.11).

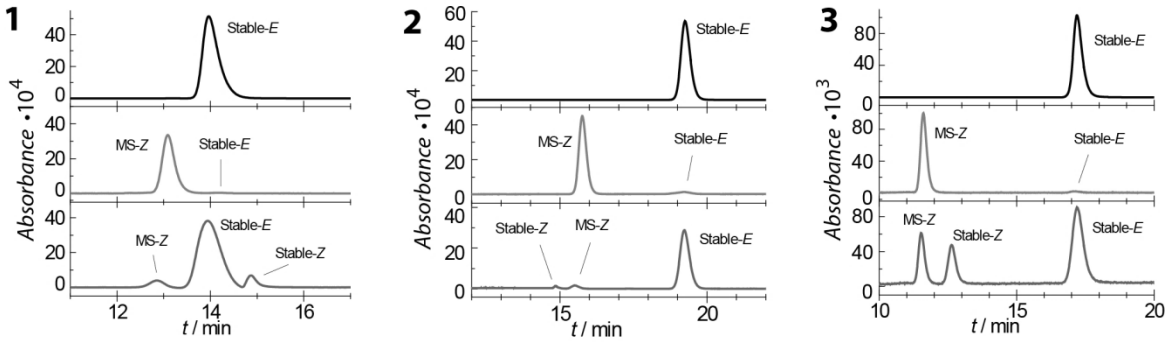

Figure 2.11. HPLC traces of (*E*)-**1**–**3**. Top: HPLC traces (heptane:2-propanol) of pure enantiomers isolated by HPLC as assigned by CD; (*E*,*M*,*R*)-**1** (Chiralcel OD-H, 98:2), (*E*,*P*,*S*)-**2** (Chiralcel AD-H, 97:3), (*E*,*M*,*R*)-**3** (Chiralcel OD-H, 98:2). Middle: HPLC traces of PSS mixtures of (*E*)-**1**–**3** (identical conditions). Bottom: HPLC traces after thermal isomerization of PSS mixtures of (*E*)-**1**–**3** (identical conditions).

Eyring analysis for each compound was performed by applying the direct Eyring equation with $1/k^2$ weighing (Figure 2.12).

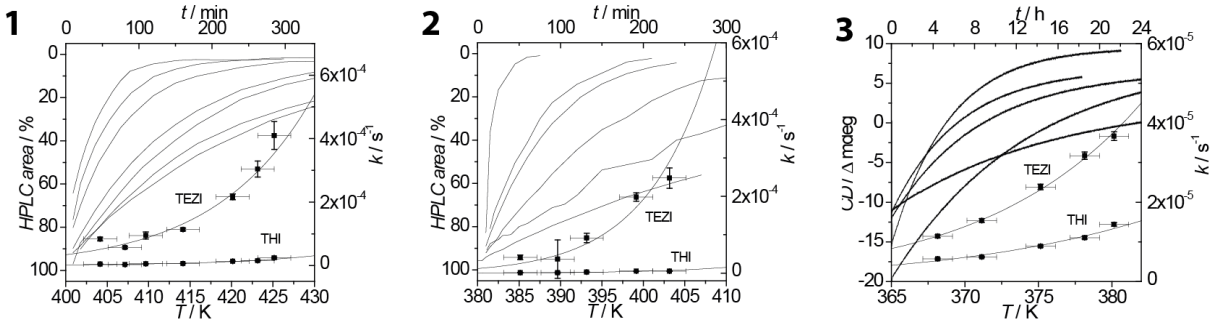

Figure 2.12. Decay curves and Eyring plots of metastable-(*Z*)-**1**–**3**. Decay curves of: (*Z*,*P*,*R*)-**1** recorded by HPLC taking aliquots from a hexanol solution (131–152 °C); (*Z*,*M*,*S*)-**2** recorded by HPLC taking aliquots from a dodecane solution (112–140 °C); (*Z*,*M*,*R*)-**3** recorded by CD in dodecane (95–107 °C). Least squares analysis on the original Eyring equation for (*E*)-**1**–**3** with error bars of 3σ.

The calculated Gibbs free energies are summarized for metastable-(*Z*)-isomers of alkenes **1**–**3** in Table 2.4. Going from carbon in **3**, to sulfur in **1** and **2**, the hour half-life temperature increases expressing a higher stability of the metastable state. Furthermore, exchanging the naphthalene moiety in **2** for the xylene moiety in **1** markedly increases the hour half-life temperature. From the Gibbs free energy of activation for the two possible pathways it is clear that under standard conditions TEZI is preferred over THI. Plotting the Gibbs free energy versus temperature (Figure 2.13), hereby assuming that the enthalpy and entropy are temperature independent, reveals also for isomers (*E*)-**1**–**3** that for the entire temperature range under investigation the barrier for the TEZI is lower than that for the THI. For alkenes (*E*)-**2** and (*E*)-**3**, the inversions points are found at experimentally relevant temperatures (-44.8 and 62.8 °C, respectively) while for (*E*)-**1** the inversion would take place below absolute zero (virtually at -399 K).

Table 2.4. Kinetic parameters determined by the direct Eyring analysis with errors obtained by a Monte Carlo experiment for thermal isomerizations of metastable (*Z*)-**1**–**3**.

	(*Z*,*P*,*R*)-**1**	(*Z*,*M*,*S*)-**2**	(*Z*,*P*,*R*)-**3**
$t_{½}$ at rt (years) [a]	$1.1±0.2·10^{3}$	$2.1±4.1·10^{4}$	11±3.8
T at $t_{½}$=1 h (°C)	144.6±0.3	126.7±0.5	122.3±0.8
$\Delta^{‡}H°_{TEZI}$ (kJ mol^{-1})	128±4.6	173±11	112±4.1
$\Delta^{‡}S°_{TEZI}$ (J K^{-1} mol^{-1})	−12.5±11	113±27	−36.3±11
$\Delta^{‡}G°_{TEZI}$ (kJ mol^{-1}) [b]	133±0.5	130±0.9	126±0.1
$\Delta^{‡}H°_{THI}$ (kJ mol^{-1})	130±4.8	156±11	87.3±3.3
$\Delta^{‡}S°_{THI}$ (J K^{-1} mol^{-1})	−31.9±12	40.9±26	−111±8.9
$\Delta^{‡}G°_{THI}$ (kJ mol^{-1}) [b]	142±0.5	141±0.9	128.6±0.1
$\Delta^{‡}H°_{total}$ (kJ mol^{-1})	128±4.6	172±11	105±3.7
$\Delta^{‡}S°_{total}$ (J K^{-1} mol^{-1})	−11.6±11	113±27	−53.3±9.8
$\Delta^{‡}G°_{total}$ (kJ mol^{-1}) [b]	133±0.5	130±0.9	125±0.05

[a] room temperature: 20 °C. [b] standard condition: 100 °C and atmospheric pressure.

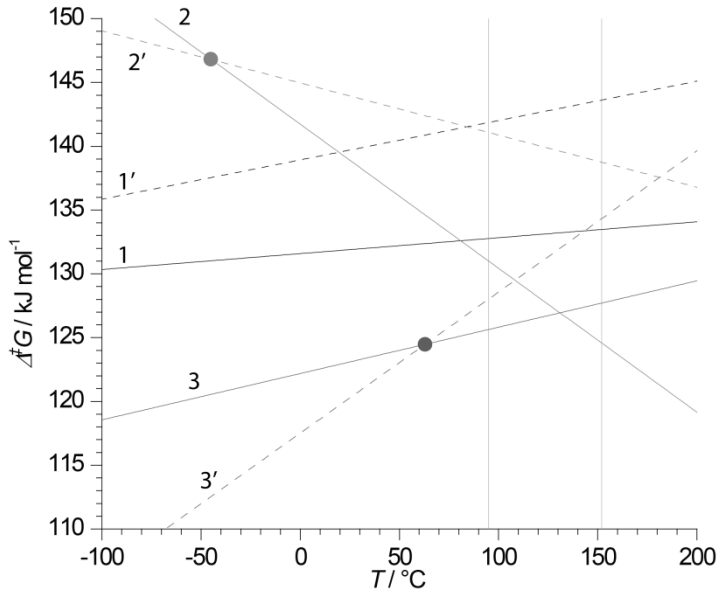

Figure 2.13. Gibbs free energy of activation for the TEZI (solid lines) and the THI (dashed lines) processes plotted vs. temperature for the metastable-(*Z*)-diastereoisomers of alkenes **1**–**3**. The experimental temperature range is marked by grey vertical lines (95–152 °C), inversion points for the two processes are marked for (*E*)-**2** and (*E*)-**3** by a dot. Inversion point for **1** falls outside measurable ranges of temperature and free Gibbs energy.

2.3 Conclusions

Four overcrowded alkenes have been synthesized and investigated experimentally and computationally. The calculated CD spectra of **1**–**4** agree well with the experimental spectra which allowed for their absolute stereochemical assignments. Irradiation with UV light allowed for high yielding *E*-*Z* isomerizations providing metastable diastereoisomers. Kinetic studies on metastable **1**–**4** using CD and HPLC identified two pathways at high temperatures for thermal isomerization. The thermal *E*-*Z* isomerizations and helix inversions were studied computationally. Furthermore, the calculated THI and TEZI barriers were found to be in close agreement with those observed experimentally. In order to show the value of these overcrowded alkenes as bistable switches, photochemical switching cycles were performed which proved the alkenes to be excellent switches. Switch **3** showed the best performance as a photo-switch while **1** excelled in thermal stability, both exhibiting highly selective isomerizations. These favorable switching properties offer attractive prospects towards the design of novel photoresponsive systems.

2.4 Acknowledgements

The author would like to thank J. C. M. Kistemaker, T. van Leeuwen and Dr. T. C. Pijper for their fundamental contribution to this work. Synthesis and characterization of **4** was performed by T. van Leeuwen and J. C. M. Kistemaker, Computational study was performed by J. C. M. Kistemaker and Dr. T. C. Pijper.

2.5 Experimental section

2.5.1 General methods

Chemicals were purchased from Sigma Aldrich, Acros or TCI Europe N.V. Solvents were reagent grade and distilled and dried before use according to standard procedures. Dichloromethane and toluene were used from the solvent purification system using an MBraun SPS-800 column. Tetrahydrofuran was distilled over sodium under a nitrogen atmosphere prior to use. Column chromatography was performed on silica gel (Silica Flash P60, 230–400 mesh). NMR spectra were recorded on a Varian Gemini-200, a Varian AMX400 or a Varian Unity Plus 500 spectrometers, operating at 200 MHz, 400 MHz, and 500 MHz for ^{1}H NMR, respectively. Chemical shifts are denoted in δ values (ppm) relative to $CDCl_3$ (^{1}H: δ = 7.26; ^{13}C: δ = 77.00). For ^{1}H NMR, the splitting parameters are designated as follows: s (singlet), d (doublet), t (triplet), q (quartet), p (pentet), sext (sextet), m (multiplet) and b (broad). MS (EI) and HRMS (EI) spectra were obtained with a AEI MS-902 or with a LTQ Orbitrap XL. Melting point are measured on a Büchi Melting Point B-545 apparatus. Preparative HPLC was performed on a Shimadzu semi-prep HPLC system consisting of an LC-20T pump, a DGU-20A degasser, a CBM-20A control module, a SIL-20AC autosampler, a SPD-M20A diode array detector and a FRC-10A fraction collector, using a Chiralpak (Daicel) AD-H, Chiralcel OD or Chiralcel OD-H column. Elution speed was 0.5 mL/min for AD-H and OD-H columns and 1.0 mL/min for the OD column, with mixtures of HPLC grade heptane and isopropanol (BOOM) as eluent. HPLC analysis was performed using a Shimadzu LC-10ADVP HPLC pump equipped with a Shimadzu SPDM10AVP diode array detector and chiral columns as indicated. Sample injections were made using an HP 6890 Series Auto sample Injector. UV-vis absorption spectra were measured on a Analityk Jena SPECORD S600 spectrophotometer. CD spectra were measured on a Jasco J-815 CD spectrophotometer. All spectra were recorded at 20 °C using Uvasol grade heptane (Merck) as solvent. Irradiation was performed using a Spectroline ENB-280C/FE lamp (312 nm, 365 nm) or a Thorlabs INC OSL 1-EC fibre illuminator (420 nm, 450 nm). Thermal helix inversion/thermal *E*—*Z* isomerization were monitored by CD spectroscopy using the apparatus described above and a JASCO PFD-350S/350L Peltier type FDCD attachment with temperature control and cooling system or by HPLC analysis of aliquots collected over time (See the Kinetic Experiments Section for further details). Temperature of oil baths during the kinetics experiments were measured with a Pt1000 RTD Temperature Sensor. Room temperature (rt) as mentioned in the experimental procedures, characterization and computational sections is to be considered equal to 20 °C.

2.5.2 Synthetic procedures

Compounds **4**, **15**, **13**, **26**, **27**, **11**, and **13** were synthesized by J. C. M. Kistemaker and T. van Leeuwen. Refer to published version of the manuscript for synthesis and full characterization.

2-methoxy-9*H*-fluoren-9-one (14)

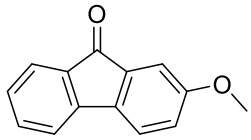

To a stirred suspension of finely powdered KOH (2.1 g, 37 mmol) in DMSO (20 mL) was added 2-hydroxy-9*H*-fluoren-9-one (2.0 g, 10 mmol) and iodomethane (2 mL, 32 mmol). The reaction suspension was stirred for 30 min. Water (50 mL) was added and the resulting mixture was extracted with Et_2O (5 x 50 mL). The organic layer was washed with H_2O (2 x 100 mL), dried over $MgSO_4$ and concentrated under reduced pressure. The obtained orange oil was purified by column chromatography (SiO_2, pentane:CH_2Cl_2 = 1:1) to yield 14 (1.97 g, 9.4 mmol, 92%) as an oil which crystallized upon standing. m.p. 78 °C; ^{1}H NMR (400 MHz, $CDCl_3$) δ 7.58 (d, *J* = 7.3 Hz, 1H), 7.44–7.35 (m, 3H), 7.23–7.14 (m, 2H), 6.96 (dd, *J* = 8.2, 2.5 Hz, 1H), 3.84 (s, 3H); ^{13}C APT NMR (100 MHz, $CDCl_3$) δ 193.8 (C), 160.8 (C), 144.8 (C), 136.9 (C), 135.9 (C), 134.8 (CH), 134.3 (C), 127.8 (CH), 124.3 (CH), 121.3 (CH), 120.2 (CH), 119.5 (CH), 109.3 (CH), 55.7 (CH_3); HRMS (APCIpos): calcd for $C_{14}H_{11}O_2$

$[M+H]^+$: 211.0759, found 211.0753; anal. calcd for $C_{14}H_{10}O_2$: C 79.98%, H 4.79%, found: C 79.90%, H 4.79%.

(*Z*) & (*E*)-2-methoxy-9*H*-fluoren-9-ylidene)hydrazine (15)

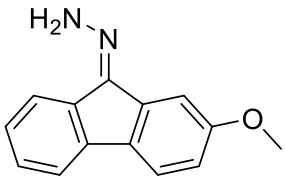

A solution of 14 (1.5 g, 7.1 mmol) and hydrazine monohydrate (3 mL) in MeOH (100 mL) was stirred and heated at reflux for 2 h. The solvent was removed under reduced pressure and the crude product was re-dissolved in CH_2Cl_2 (50 mL). The organic phase was extracted with H_2O (2 x 50 mL) and dried over Na_2SO_4. The crude product was purified by column chromatography (SiO_2, solvent gradient: pentane:EtOAc = 1:0 to 1:1) to yield 15 (1.3 g, 5.8 mmol, 82%) as a yellow solid. ^{1}H NMR (400 MHz, $CDCl_3$) δ 7.78–7.67 (m, 2H), 7.61–7.41 (m, 5H), 7.41–7.13 (m, 7H), 6.86 (dt, *J* = 8.3, 2.4 Hz, 2H), 6.37 (d, *J* = 14.0 Hz, 2H), 3.84 (s, 3H), 3.79 (d, *J* = 2.4 Hz, 3H); ^{13}C APT NMR (100 MHz, $CDCl_3$) δ 160.3 (C), 159.8 (C), 145.6 (C), 145.4 (C), 141.6 (C), 139.8 (C), 138.9 (C), 137.8 (C), 134.3 (C), 131.8 (C), 131.6 (C), 130.4 (C), 129.9 (CH), 128.7 (CH), 126.9 (CH), 126.7 (CH), 125.5 (CH), 121.2 (CH), 120.8 (CH), 120.7 (CH), 119.8 (CH), 119.0 (CH), 115.6 (CH), 114.1 (CH), 112.8 (CH), 105.4 (CH), 55.8 (CH_3), 55.8 (CH_3); HRMS (APCIpos): calcd for $C_{14}H_{13}N_2O$ $[M+H]^+$: 225.10224, found 225.1026.

3,5,8-trimethylthiochroman-4-one (7)

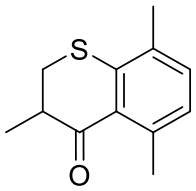

A solution of 2-(2,5-dimethylphenyl)thiol (2.00 g, 14.5 mmol), NEt_3 (4.00 mL, 28.9 mmol) and methacrylic acid (2.45 mL, 28.9 mmol) in THF (25 mL) was heated at reflux under stirring for 16 h. Upon cooling, the reaction mixture was quenched with aq. 1M HCl (30 mL) and the water layer was extracted with EtOAc (3 × 30 mL). The combined organic layers were washed with brine and dried over Na_2SO_4. After filtration, the volatiles were removed under reduced pressure and the crude 3-((2,5-dimethylphenyl)thio)-2-methylpropanoic acid **5** was obtained as a light brown solid (3.20 g, 14.4 mmol). Despite minor impurities, the crude product was used directly in the following step. A round-bottom flask equipped with a septa-cap pierced with a needle was loaded with a solution of **5** (3.20 g, 14.4 mmol) and two drops of DMF in CH_2Cl_2 (20 mL). Oxalyl chloride (2.50 mL, 28.50 mmol) was slowly added to the solution dropwise, which turned from yellow to orange. The solution was stirred for 1 h at rt, then the volatiles were removed under reduced pressure. Heptane (15 mL) was added and the solvent evaporated under reduced pressure at 60 °C twice to remove completely the excess of oxalyl chloride, to yield the crude 3-((2,5-dimethylphenyl)thio)-2-methylpropanoyl chloride **6** (3.44 g, 14.2 mmol) as a brownish oil. The crude product was used directly in the following step without further purification. Under a nitrogen atmosphere, **6** (4.10 g, 15.5 mmol) was re-dissolved in CH_2Cl_2 (70 mL) and cooled to 0 °C. $AlCl_3$ (2.64 g, 19.8 mmol) was slowly added to the solution portionwise to avoid heating of the mixture. The mixture was stirred for 2 h at low temperature. Subsequently, the mixture was warmed up and quenched with aq. 1M HCl (50 mL) in an ice bath. The organic phase was separated and the aqueous phase was extracted with CH_2Cl_2 (3 x 30 mL). The organic phases were combined and washed with brine and dried over Na_2SO_4. After filtration, the volatiles were removed under reduced pressure and the crude product was purified by column chromatography (SiO_2, pentane:EtOAc = 20:1, R_f = 0.30) to yield **7** (2.40 g, 11.6 mmol, 80% from the initial 2-(2,5-dimethylphenyl)thiol) as a light yellow oil. ^{1}H NMR (200 MHz, $CDCl_3$) δ 7.11 (d, *J* = 7.6 Hz, 1H), 6.88 (d, *J* = 7.6 Hz, 1H), 3.26–2.81 (m, 4H), 2.54 (s, 3H), 2.27 (s, 3H), 1.31 (d, *J* = 6.2 Hz, 3H); ^{13}C NMR (50 MHz, $CDCl_3$) δ 199.8, 141.4, 139.7, 132.8, 132.6, 130.2, 128.0, 42.8, 32.2, 23.4, 19.9, 15.2; HRMS (ESI, m/z): calcd for $C_{12}H_{15}OS$ $[M+H]^+$: 207.0838, found: 207.0838.

(3,5,8-trimethylthiochroman-4-ylidene)hydrazine (8)

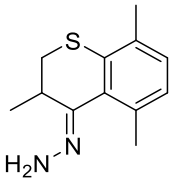

Under a nitrogen atmosphere, a mixture of **7** (1.25 g, 6.06 mmol), hydrazine monohydrate (4 mL) and $Sc(OTf)_3$ (0.075 g, 0.151 mmol, 2.5 mol%) in EtOH (4 mL) was heated at reflux for 16 h. The solution was allowed to cool to rt and water was added under stirring until the product started precipitating. The mixture was cooled to −25 °C for 16 h. The slurry was filtered on a P4 fritted glass filter, the solid residue was washed with cold Et_2O and cold pentane and dried under *vacuo* to yield **8** (0.90 g, 4.08 mmol, 67%) as white powder. m.p. 123–124 °C; ^{1}H NMR (400 MHz, $CDCl_3$) δ 7.04–6.90 (m, 2H), 5.40 (s, 2H), 3.46–3.31 (m, 1H), 3.06 (dd, *J* = 12.9, 6.4 Hz, 1H), 2.53 (dd, *J* = 12.9, 10.4 Hz, 1H), 2.39 (s, 3H), 2.28 (d, *J* = 7.8 Hz, 3H), 1.22 (d, *J* = 6.8 Hz, 3H); ^{13}C NMR (50 MHz, $CDCl_3$) δ 150.8, 137.9, 135.3, 134.5, 133.3, 128.7, 128.3, 36.4, 34.5, 21.0, 19.9, 14.9; HRMS (APCI, m/z): calcd for $C_{12}H_{17}N_2S$ $[M+H]^+$: 221.1107, found: 221.1107.

(*Z*) & (*E*)-4-(2-methoxy-9*H*-fluoren-9-ylidene)-3,5,8-trimethylthiochromane (1)

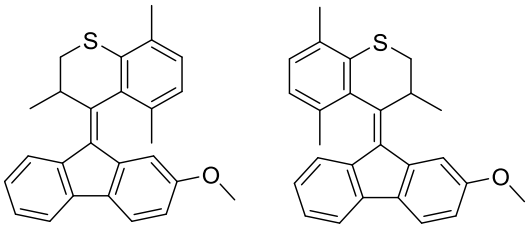

Under a nitrogen atmosphere, Lawesson's reagent (1.38 g, 3.4 mmol) was added to a stirred solution of **14** (480 mg, 2.27 mmol) in dry toluene (6 mL). The mixture was heated at 90 ºC for approximately 1 h, until TLC (pentane:CH_2Cl_2 = 2:1) started showing the formation of degradation products. The mixture was concentrated and the residue was purified by quick column chromatography (SiO_2, pentane:CH_2Cl_2 = 2:1). The wine red fraction was concentrated under reduced pressure to yield the crude thioketone **12** as a dark wine red oil (to prevent hydrolysis, the product was kept wet with CH_2Cl_2 and stored under nitrogen). Under a nitrogen atmosphere, a solution of **8** (500 mg, 2.27 mmol) in DMF (4 mL) was cooled to −40 °C and bis(trifluoroacethoxy)iodobenzene (920 mg, 2.27 mmol) was added to the stirred solution. The mixture was stirred for 2 min while the color turned from yellow to dark pink, indicative of the formation *in situ* of the diazo compound **16**. A solution of the crude thioketone **12** in dry DMF (4 mL) and dry of CH_2Cl_2 (4 mL) was added to the mixture, which showed evolution of nitrogen gas. The mixture was allowed to warm to rt and stirred for 16 h. The mixture was diluted with EtOAc, washed with a sat. aq. NH_4Cl solution, the organic layer was separated and the aqueous layer was extracted with EtOAc (3 x 10 mL). The organic phases were collected, washed with water, brine and dried over Na_2SO_4. After filtration, the volatiles were removed under reduced pressure and the crude residue was re-dissolved in toluene (8 mL). Tris(dimethylamino)phosphine (0.32 mL, 1.74 mmol) was added and the mixture was stirred for 16 h at 65 °C. The mixture was concentrated under reduced pressure and the crude product was re-dissolved in CH_2Cl_2 (15 mL), washed with water, brine and dried over Na_2SO_4. After filtration, the volatiles were removed under reduced pressure and the crude product was purified by column chromatography (SiO_2, solvent gradient: pentane:EtOAc = 50:1 to 20:1) to yield (*Z*)-**1** (180 mg, 0.46 mmol, 21%) and (*E*)-**1** (190 mg, 0.49 mmol, 22%) as yellow crystals (*Z*:*E* = 1:1.1).

(*Z*)-**1**: m.p. 168–169 °C; ^{1}H NMR (400 MHz, $CDCl_3$) δ 7.90 (d, *J* = 7.7 Hz, 1H), 7.65 (d, *J* = 7.4 Hz, 1H), 7.51 (d, *J* = 8.3 Hz, 1H), 7.34 (td, *J* = 7.4, 0.9 Hz, 1H), 7.27 (td, *J* = 7.7, 1.3 Hz, 1H), 7.17 (d, *J* = 7.7 Hz, 1H), 7.05 (d, *J* = 7.7 Hz, 1H), 6.75 (dd, *J* = 8.3, 2.4 Hz, 1H), 5.88 (d, *J* = 2.3 Hz, 1H), 4.54 (app. sext, *J* = 7.4 Hz, 1H), 3.42 (s, 3H), 3.22 (dd, *J* = 12.6, 7.8 Hz, 1H), 2.42 (s, 3H), 2.35 (dd, *J* = 12.5, 8.8 Hz, 1H), 2.18 (s, 3H), 1.38 (d, *J* = 6.8 Hz, 3H); ^{13}C NMR (50 MHz, $CDCl_3$) δ 159.2, 144.6, 141.3, 139.8, 139.2, 137.6, 136.0, 135.1, 132.9, 132.8, 129.1, 128.0, 127.6, 125.8, 124.8, 119.6, 118.8, 114.8, 107.8, 55.0, 40.2, 37.1, 19.9, 19.7, 18.8, one signal (C) was not observed; HRMS (ESI, m/z): calcd for $C_{26}H_{25}OS$ $[M+H]^+$: 385.1621, found: 385.1617. Separation of the enantiomers was achieved by CSP-HPLC (Chiralcel OD-H, heptane:2-propanol = 98:2, flow rate = 0.5 mL/min, Rt: 17.40 min for (*Z*,*P*,*S*)-**1**, 26.40 min for (*Z*,*M*,*R*)-**1**.

(*E*)-**1**: m.p. 159–161 °C; ^{1}H NMR (400 MHz, $CDCl_3$) δ 7.66 (d, *J* = 8.3 Hz, 1H), 7.55 (d, *J* = 7.6 Hz, 1H), 7.52 (d, *J* = 2.0 Hz, 1H), 7.18 (d, *J* = 7.7 Hz, 1H), 7.15 (t, *J* = 7.5 Hz, 1H), 7.02 (d, *J* = 7.7 Hz, 1H), 6.95

(dd, *J* = 8.3, 2.2 Hz, 1H), 6.80 (t, *J* = 7.7 Hz, 1H), 6.22 (d, *J* = 8.0, 1H), 4.51 (app. sext, *J* = 7.6 Hz, 1H), 3.93 (s, 3H), 3.22 (dd, *J* = 12.5, 7.8 Hz, 1H), 2.42 (s, 3H), 2.35 (dd, *J* = 12.5, 8.7 Hz, 1H), 2.13 (s, 3H), 1.37 (d, *J* = 6.8 Hz, 3H); ^{13}C NMR (50 MHz, $CDCl_3$) δ 159.2, 144.6, 139.6, 139.3, 138.9, 138.26, 137.6, 135.9, 134.9, 134.3, 132.9, 129.2, 128.1, 127.4, 126.1, 123.3, 120.1, 118.2, 112.2, 112.1, 55.7, 39.9, 37.1, 20.0, 19.7, 18.6; HRMS (ESI, m/z): calcd for $C_{26}H_{25}OS$ $[M+H]^+$: 385.1621, found: 385.1616. Separation of the enantiomers was achieved by CSP-HPLC (Chiralcel OD-H, heptane:2-propanol = 98:2, flow rate = 0.5 mL/min, Rt: 16.60 min for (*E*,*M*,*R*)-**1**, 23.00 min for (*E*,*P*,*S*)-**1**.

3-((naphthalen-2-yl)thio)-2-methylpropanoic acid (18)

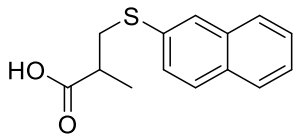

A solution of naphthalen-2-thiol (5.0 g, 31.2 mmol), NEt_3 (8.70 mL, 62.4 mmol) and methacrylic acid (5.30 mL, 62.4 mmol) in THF (50 mL) was heated at reflux under stirring for 16 h. Upon cooling, the reaction mixture was quenched with aq. 1M HCl (40 mL) and the water layer was extracted with EtOAc (3 x 30 mL). The combined organic layers were washed with brine and dried over Na_2SO_4. After filtration, the volatiles were removed under reduced pressure and the crude product was purified by recrystallization from heptane to yield **18** (5.65 g, 22.9 mmol, 73%) as a white powder. m.p. 88–89 °C; ^{1}H NMR (200 MHz, $CDCl_3$) δ 7.84–7.72 (m, 3H), 7.53–7.35 (m, 2H), 3.39 (dd, *J* = 13.4, 6.9 Hz, 1H), 3.02 (dd, *J* = 13.4, 7.0 Hz, 1H), 2.76 (ddd, *J* = 13.9, 7.0, 6.9 Hz, 1H), 1.33 (d, *J* = 7.0 Hz, 3H); ^{13}C NMR (75 MHz, $CDCl_3$) δ 181.3, 133.7, 132.8, 132.0, 128.6, 128.3, 127.9, 127.7, 127.2, 126.6, 125.9, 39.4, 37.0, 16.5; HRMS (ESI, m/z): calcd for $C_{14}H_{15}O_2S$ $[M+H]^+$: 247.0787, found: 247.0793.

2,3-dihydro-2-methyl-1*H*-naphtho[2,1-b]thiopyran-1-one (20)

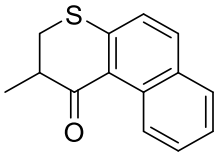

A round-bottom flask equipped with a septa-cap pierced with a needle was loaded with a solution of **18** (3.80 g, 15.5 mmol) and two drops of DMF in CH_2Cl_2 (60 mL). Oxalyl chloride (6.32 mL, 31.0 mmol) was slowly added to the solution dropwise, liberating gas and the solution turned from yellow to orange. The solution was stirred for 1 h at rt, then the volatiles were removed under reduced pressure. Heptane (15 mL) was added and the solvent evaporated under reduced pressure at 60 °C twice to remove completely the excess of oxalyl chloride, to yield the crude 2-methyl-3-(naphthalen-2-ylthio)propanoyl chloride **19** (4.10 g, 15.5 mmol) as a brownish oil. The product was used immediately in the following step without further purification. Under a nitrogen atmosphere, **19** was re-dissolved in CH_2Cl_2 (60 mL) and the mixture cooled to −50 °C. $AlCl_3$ (3.10 g, 23.2 mmol) was slowly added to the solution portionwise to avoid heating of the mixture. The mixture was stirred for 2 h, then it was let to warm to rt and quenched with aq. 1M HCl (40 mL)in an ice bath. The organic phase was separated and the aqueous phase was extracted with CH_2Cl_2 (3 x 30 mL). The combined organic phases were combined and washed with brine and dried over Na_2SO_4. After filtration, the volatiles were removed under reduced pressure and the crude product was purified by column chromatography (SiO_2, pentane:EtOAc 5:1, R_f = 0.40) to yield **20** (2.62 g, 11.5 mmol, 75%) as an orange oil. ^{1}H NMR (400 MHz, $CDCl_3$) δ 9.07 (dq, *J* = 8.8, 0.9 Hz, 1H), 7.82–7.70 (m, 2H), 7.58 (ddd, *J* = 8.6, 6.8, 1.5 Hz, 1H), 7.44 (ddd, *J* = 8.0, 6.9, 1.2 Hz, 1H), 7.24 (d, *J* = 8.7 Hz, 1H), 3.30–3.06 (m, 3H), 1.40 (d, *J* = 6.6 Hz, 3H); ^{13}C NMR (75 MHz, $CDCl_3$) δ 199.2, 143.9, 133.2, 132.4, 131.6, 128.9, 128.4, 125.6, 125.5, 125.3, 125.0, 42.8, 32.8, 15.3. The data were identical in all respects to those previously reported.[64]

(2-methyl-2,3-dihydro-1*H*-benzo[*f*]thiochromen-1-ylidene)hydrazine (9)

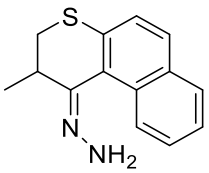

Under a nitrogen atmosphere, a mixture of **20** (780 mg, 3.42 mmol) and hydrazine monohydrate (2 mL) in EtOH (2 mL) was heated at reflux for 16 h. When full conversion was reached — monitored by TLC (pentane:CH_2Cl_2 = 6:1) — the heating was stopped and the solution was allowed to cool to rt without stirring over 3 h. Part of the product precipitated as light-yellow crystals. After separation from the liquid phase, the crystals were washed with cold Et_2O, dissolved in CH_2Cl_2, dried over

Na_2SO_4 and, after filtration, the volatiles were removed under reduced pressure. The liquid phase was diluted with CH_2Cl_2 (20 mL) and washed with water (3 x 20 mL), brine and dried over Na_2SO_4. After filtration, the volatiles were removed under reduced pressure and the crude product was purified by column chromatography (SiO_2, solvent gradient: pentane:EtOAc:NEt_3 = 80:15:5 to 30:65:5) to yield **9** (combined collected fractions: 0.56 g, 2.31 mmol, 68%) as light yellow crystals. ^{1}H NMR (400 MHz, $CDCl_3$) δ 8.42 (d, *J* = 8.4 Hz, 1H), 7.76 (d, *J* = 8.2 Hz, 1H), 7.64 (d, *J* = 8.5 Hz, 1H), 7.48 (ddd, *J* = 8.6, 6.9, 1.6 Hz, 1H), 7.40 (ddd, *J* = 8.0, 6.8, 1.3 Hz, 1H), 7.34 (d, *J* = 8.5 Hz, 1H), 3.61–3.49 (m, 1H), 3.20 (ddd, *J* = 12.8, 5.9, 2.2 Hz, 1H), 2.71 (ddd, *J* = 12.8, 9.7, 2.4 Hz, 1H), 1.33 (d, *J* = 6.8 Hz, 3H); ^{13}C NMR (75 MHz, $CDCl_3$) δ 149.3, 135.7, 133.0, 132.1, 130.8, 128.0, 127.7, 126.7, 126.1, 125.9, 125.1, 36.4, 34.0, 14.7. The data were identical in all respects to those previously reported.[65]

(*Z*) & (*E*)-1-(2-Methoxy-9*H*-fluoren-9-ylidene)-2-methyl-1,2-dihydro-1*H*-benzo[*f*]thiocromene (2)

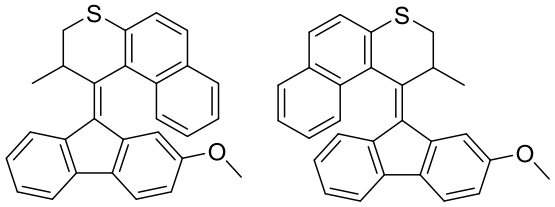

Under a nitrogen atmosphere, Lawesson's reagent (1.00 g, 2.55 mmol) was added to a stirred solution of **14** (360 mg, 1.71 mmol) in dry toluene (5 mL). The mixture was heated at 90 ºC for approximately 1 h, until TLC (pentane:CH_2Cl_2 = 2:1) started showing the formation of degradation products. The mixture was concentrated and the residue was purified by quick column chromatography (SiO_2, pentane:CH_2Cl_2 = 2:1). The wine red fraction was concentrated under reduced pressure to yield the crude thioketone **12** as a dark wine red oil (to prevent hydrolysis, the product was kept wet with CH_2Cl_2 and stored under a nitrogen atmosphere). Under a nitrogen atmosphere, a solution of **9** (280 mg, 1.154 mmol) in DMF (6 mL) was cooled to −40 °C and bis(trifluoroacethoxy)iodobenzene (248 mg, 1.154 mmol) was added to the stirred solution. The mixture was stirred for 1 min while the color turned from yellow to dark pink, indicative of the formation *in situ* of the diazo compound **21**. A solution of the crude thioketone **12** in dry DMF (1 mL) and dry CH_2Cl_2 (1 mL) was added to the mixture, which showed the evolution of nitrogen gas. The mixture was allowed to warm to rt and stirred for 2 h. The mixture was diluted with EtOAc, washed with a sat. aq. NH_4Cl solution, the organic layer was separated and the aqueous layer was extracted with EtOAc (3 x 10 mL). The organic phases were collected, washed with water, brine and dried over Na_2SO_4. After filtration, the volatiles were removed under reduced pressure and the crude product was purified by column chromatography (SiO_2, pentane:EtOAc = 50:1, R_f ((*Z*)-**22**) = 0.40, R_f ((*E*)-**22**) = 0.30) to yield yield (*Z*)-**22** (113 mg, 0.28 mmol, 24%) and (*E*)-**22** (147 mg, 0.36 mmol, 31%) as yellow amorphous residues (*Z*:*E* = 1:1.3).

(*Z*)-**22:** ^{1}H NMR (400 MHz, $CDCl_3$) δ 8.84 (d, *J* = 8.7 Hz, 1H), 7.82 (d, *J* = 8.1 Hz, 1H), 7.65 (d, *J* = 7.5 Hz, 1H), 7.63–7.57 (m, 3H), 7.51–7.44 (m, 2H), 7.37 (t, *J* = 7.4 Hz, 1H), 7.23 (t, *J* = 7.5 Hz, 1H), 7.12 (d, *J* = 8.4 Hz, 1H), 6.63 (dd, *J* = 8.3, 2.4 Hz, 1H), 5.04 (d, *J* = 2.3 Hz, 1H), 3.73–3.61 (m, 1H), 2.83 (s, 3H), 2.74 (dd, *J* = 12.1, 10.1 Hz, 1H), 2.43 (dd, *J* = 12.1, 5.1 Hz, 1H), 1.24 (d, *J* = 6.9 Hz, 3H).

(*E*)-**22:** ^{1}H NMR (400 MHz, $CDCl_3$) δ 8.78 (d, *J* = 8.9 Hz, 1H), 7.85 (d, *J* = 8.1 Hz, 1H), 7.66 (d, *J* = 8.3 Hz, 1H), 7.62–7.57 (m, 2H), 7.50 (d, *J* = 7.4 Hz, 2H), 7.19 (d, *J* = 2.2 Hz, 1H), 7.06 (d, *J* = 8.5 Hz, 1H), 7.05 (t, *J* = 7.5 Hz, 1H), 6.95 (dd, *J* = 8.3, 2.3 Hz, 1H), 6.39 (t, *J* = 7.6 Hz, 1H), 5.37 (d, *J* = 7.8 Hz, 1H), 3.91 (s, 3H), 3.69–3.57 (m, 1H), 2.77 (dd, *J* = 12.1, 10.0 Hz, 1H), 2.40 (dd, *J* = 12.2, 5.3 Hz, 1H), 1.22 (d, *J* = 6.9 Hz, 3H).

A solution of (*Z*)-**22** (59 mg, 0.134 mmol) and tris(dimethylamino)phosphine (0.05 mL, 0.27 mmol) in toluene (3 mL) was stirred for 16 h at 65 °C. The mixture was then concentrated under reduced pressure and the crude product was re-dissolved in CH_2Cl_2, washed with water, brine and dried over Na_2SO_4. After filtration, the volatiles were removed under reduced pressure and the crude product was purified by column chromatography (SiO_2, solvent gradient: pentane:EtOAc = 100:1 to 50:1) to yield (*Z*)-**2** (52 mg, 0.13 mmol, 95% from (*Z*)-**22**, 22% from **9**) as yellow needles. (*Z*)-**2**: m.p. 191–192 °C; ^{1}H NMR (500 MHz, $CDCl_3$) δ 8.02 (d, *J* = 7.7 Hz, 1H), 7.91 (d, *J* = 8.6 Hz, 1H), 7.82 (t, *J* = 8.5 Hz, 2H), 7.65 (d, *J* = 6.8 Hz, 1H), 7.60 (d,

J = 8.5 Hz, 1H), 7.44 (d, *J* = 8.3 Hz, 1H), 7.40–7.35 (m, 2H), 7.34–7.29 (m, 1H), 7.28–7.22 (m, 1H), 6.60 (dd, *J* = 8.3, 2.3 Hz, 1H), 5.25 (d, *J* = 2.3 Hz, 1H), 4.77 (ddd, *J* = 7.8, 7.3, 6.8 Hz, 1H), 3.36 (dd, *J* = 12.3, 7.3 Hz, 1H), 2.88 (s, 3H), 2.59 (dd, *J* = 12.3, 7.8 Hz, 1H), 1.41 (d, *J* = 6.8 Hz, 3H); ^{13}C NMR (126 MHz, $CDCl_3$) δ 158.6, 142.1, 141.5, 138.9, 137.5, 137.3, 134.3, 134.1, 133.4, 133.0, 132.2, 128.0, 127.9, 127.6, 127.5, 125.8, 125.6, 125.1, 124.8, 119.5, 118.9, 115.4, 108.9, 54.4, 39.5, 37.4, 18.7, one signal (C) was not observed; HRMS (ESI, m/z): calcd for $C_{28}H_{23}OS$ $[M+H]^+$: 407.1464, found: 407.1466. Separation of the enantiomers was achieved by CSP-HPLC (Chiralpak AD-H, heptane:2-propanol = 97:3, flow rate = 0.5 mL/min, Rt: 14.5 min for (*Z*,*P*,*S*)-**2**, 21.8 min for (*Z*,*M*,*R*)-**2**.

Following the same methodology, (*E*)-**22** (60 mg, 0.134 mmol) was treated with tris(dimethylamino)phosphine (0.05 mL, 0.27 mmol) in toluene (3 mL), to yield (*E*)-**2** (52 mg, 0.13 mmol, 95% from (*E*)-**22**, 22% from **9**) as yellow needles.

(*E*)-**2:** m.p. 243–244 °C; ^{1}H NMR (500 MHz, $CDCl_3$) δ 7.85 (t, *J* = 7.4 Hz, 3H), 7.71–7.62 (m, 2H), 7.58 (d, *J* = 8.6 Hz, 1H), 7.49 (d, *J* = 7.4 Hz, 1H), 7.36 (t, *J* = 7.5 Hz, 1H), 7.21 (t, *J* = 7.7 Hz, 1H), 7.03–6.93 (m, 2H), 6.46 (t, *J* = 7.7 Hz, 1H), 5.65 (d, *J* = 8.0 Hz, 1H), 4.73 (ddd, *J* = 7.7, 7.3, 6.8, Hz 1H), 3.96 (s, 3H), 3.35 (dd, *J* = 12.2, 7. Hz 3, 1H), 2.59 (dd, *J* = 12.2, 7.7 Hz, 1H), 1.38 (d, *J* = 6.8 Hz, 3H); ^{13}C NMR (126 MHz, $CDCl_3$) δ 159.3, 142.2, 139.7, 139.3, 137.4, 136.8, 134.6, 134.2, 134.1, 133.3, 132.1, 128.3, 128.1, 127.3, 127.2, 127.2, 125.6, 125.4, 124.9, 124.6, 120.2, 118.1, 112.6, 112.3, 55.8, 39.1, 37.3, 18.5; HRMS (ESI, m/z): calcd for $C_{28}H_{23}OS$ $[M+H]^+$: 407.1464, found: 407.1465. Separation of the enantiomers was achieved by CSP-HPLC (Chiralpak AD-H, heptane:2-propanol = 97:3, flow rate = 0.5 mL/min, 40 ºC. Rt: 19.4 min for (*E*,*P*,*S*)-**2**, 22.9 min for (*E*,*P*,*R*)-**2**.

3-methyl-2,3-dihydrophenanthren-4(1*H*)-one (23)

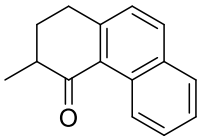

Compound **23** was prepared from 2,3-dihydrophenanthren-4(1*H*)-one by following the procedure previously reported (320 mg, 1.52 mmol, 96%). Analytical data were in accord with the literature.[66] ^{1}H NMR (400 MHz, $CDCl_3$) δ 9.34 (d, *J* = 8.7 Hz, 1H), 7.90 (d, *J* = 8.4 Hz, 1H), 7.80 (dd, *J* = 8.1, 1.4 Hz, 1H), 7.61 (ddd, *J* = 8.7, 7.0, 1.4 Hz, 1H), 7.48 (ddd, *J* = 8.1, 7.0, 1.1 Hz, 1H), 7.29 (d, *J* = 8.4 Hz, 1H), 3.21 (ddd, *J* = 17.4, 10.8, 5.0 Hz, 1H), 3.15 (ddd, *J* = 17.4, 4.8, 4.5 Hz, 1H), 2.77 (ddq, *J* = 11.9, 6.8, 4.7 Hz, 1H), 2.27 (dddd, *J* = 12.9, 11.9, 10.4, 4.7 Hz, 1H), 1.99 (dddd, *J* = 12.9, 5.0, 4.7, 4.5 Hz, 1 H), 1.32 (d, *J* = 6.8 Hz, 3 H); ^{13}C NMR (100 MHz, $CDC1_3$) δ 203.1, 145.6, 133.5, 132.5, 131.1, 128.3, 128.0, 126.9, 126.7, 126.3, 125.5, 43.6, 30.9, 30.1, 15.7.

(3-methyl-2,3-dihydrophenanthren-4(1H)-ylidene)hydrazine (10)

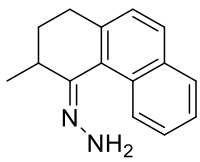

Compound **10** was prepared starting from **23** (320 mg, 1.52 mmol) by following the procedure previously reported (226 mg, 1.01 mmol, 67%). Analytical data were in accord with the literature.[64] ^{1}H NMR (400 MHz, $CDCl_3$) δ 8.78 (d, *J* = 8.4 Hz, 1H), 7.78 (d, *J* = 7.5 Hz, 1H), 7.69 (d, *J* = 8.2 Hz, 1H), 7.52–7.45 (m, 1H), 7.40 (app. t, *J* = 7.4 Hz, 1H), 7.24 (d, *J* = 8.3 Hz, 1H), 3.24–3.13 (m, 1H), 2.82 (dt, *J* = 15.3, 4.3 Hz, 1H), 2.68 (ddd, *J* = 15.3, 11.8, 3.9 Hz, 1H), 2.36–2.25 (m, 1H), 1.50–1.29 (m, 1H), 1.27 (d, *J* = 6.9 Hz, 3H); ^{13}C NMR (126 MHz, $CDCl_3$) δ 151.7, 138.9, 133.4, 131.0, 129.9, 128.0, 128.0, 126.4, 126.4, 126.0, 124.8, 31.7, 29.7, 29.5, 16.1.

(*Z*) & (*E*)-4-(2-methoxy-9*H*-fluoren-9-ylidene)-3-methyl-1,2,3,4-tetrahydrophenanthrene (3)

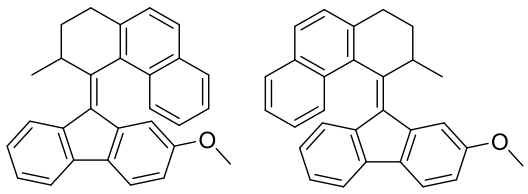

Under a nitrogen atmosphere, Lawesson's reagent (810 mg, 2.00 mmol) was added to a stirred solution of **14** (280 mg, 1.33 mmol) in dry toluene (4 mL). The mixture was heated at 90 ºC for approximately 1 h, until TLC (pentane:CH_2Cl_2 = 2:1) started showing the formation of degradation products. The mixture was concentrated and

the residue was purified by quick column chromatography (SiO_2, pentane:CH_2Cl_2 2:1). The wine red fraction was concentrated under reduced pressure to yield the crude thioketone **12** as a dark wine red oil (to prevent hydrolysis, the product was kept wet with CH_2Cl_2 and stored under a nitrogen atmosphere). Under a nitrogen atmosphere, a solution of **10** (180 mg, 0.80 mmol) in DMF (4 mL) was cooled to –40 °C and bis(trifluoroacethoxy)iodobenzene (384 mg, 0.90 mmol) was added to the stirred solution. The mixture was stirred for 1 min while the color turned from yellow to dark pink, indicative of the formation *in situ* of the diazo compound **24**. A solution of the crude thioketone **12** in dry DMF (2 mL) and dry of CH_2Cl_2 (2 mL) was added to the mixture, which showed the evolution of nitrogen gas. The mixture was allowed to warm to rt and stirred for 16 h. The mixture was diluted with EtOAc, washed with a sat. aq. NH_4Cl solution, the organic layer was separated and the aqueous layer was extracted with EtOAc (3 x 10 mL). The organic phases were collected, washed with water, brine and dried over Na_2SO_4. After filtration, the volatiles were removed under reduced pressure and the crude product was purified by column chromatography (SiO_2, pentane:EtOAc = 50:1) to yield a mixture of episulfides **25** (220 mg, 0.52 mmol, 65%, *Z*:*E* = 1:1) as a yellow amorphous residue. (*Z*)-**25**: ^{1}H NMR (200 MHz, $CDCl_3$) δ 9.18 (d, *J* = 8.6 Hz, 1H), 7.83 (d, *J* = 8.1 Hz, 1H), 7.74–7.51 (m, 4H), 7.51–7.33 (m, 3H), 7.26 (t, *J* = 7.5 Hz, 1H), 6.98 (d, *J* = 8.2 Hz, 1H), 6.61 (dd, *J* = 8.3, 2.4 Hz, 1H), 5.46 (d, *J* = 2.4 Hz, 1H), 3.20–3.05 (m, 1H), 2.71 (s, 3H), 2.18 (dd, *J* = 14.6, 5.3 Hz, 1H), 1.95–1.80 (m, 1H), 1.75–1.53 (m, 1H), 1.11 (d, *J* = 6.9 Hz, 3H), 1.1–0.95 (m, 1H). (*E*)-**25:** ^{1}H NMR (400 MHz, $CDCl_3$) δ 9.10 (d, *J* = 8.7 Hz, 1H), 7.84 (d, *J* = 9.9 Hz, 1H), 7.67–7.55 (m, 3H), 7.48 (d, *J* = 8.5 Hz, 2H), 7.24 (d, *J* = 2.3 Hz, 1H), 7.03 (t, *J* = 7.0 Hz, 1H), 6.97 (dd, *J* = 8.3, 2.3 Hz, 1H), 6.94 (d, *J* = 8.2 Hz, 1H), 6.41 (t, *J* = 7.1 Hz, 1H), 5.76 (d, *J* = 7.8 Hz, 1H), 3.92 (s, 3H), 3.14–3.04 (m, 1H), 2.16 (dd, *J* = 14.6, 5.1 Hz, 1H), 1.93–1.82 (m, 1H), 1.72–1.57 (m, 1H), 1.07 (d, *J* = 6.9 Hz, 3H), 1.05–0.95 (m, 1H).
The mixture of (*Z*)- and (*E*)-**25** was re-dissolved in toluene (15 mL), tris(dimethylamino)phosphine (0.29 mL, 1.60 mmol) was added and the mixture was stirred for 16 h at rt. The mixture was concentrated under reduced pressure and the residue was re-dissolved in CH_2Cl_2 (15 mL), washed with water (2 x 15 mL), brine and dried over Na_2SO_4. After filtration, the volatiles were removed under reduced pressure and the crude product was purified by column chromatography (SiO_2, pentane:EtOAc = 50:1) to yield (*Z*)-**3** (98.1 mg, 0.25 mmol, 48% from mixture of (*Z*)- and (*E*)-**25**, 30% from **10**) and (*E*)-**3** (104.2 mg, 0.27 mmol, 51% from mixture of (*Z*) & (*E*)-**25**, 32% from **10**) as yellow needles. (*Z*)-**3**: m.p. 174–175 °C; ^{1}H NMR (500 MHz, $CDCl_3$) δ 8.05 (d, *J* = 7.7 Hz, 1H), 7.97 (d, *J* = 8.5 Hz, 1H), 7.85 (d, *J* = 8.3 Hz, 2H), 7.69 (d, *J* = 7.1 Hz, 1H), 7.47 (t, *J* = 8.0 Hz, 2H), 7.37 (t, *J* = 7.4 Hz, 2H), 7.33 (dt, *J* = 7.5, 3.8 Hz, 1H), 7.25 (dt, *J* = 8.1, 2.0 Hz, 1H), 6.62 (dd, *J* = 8.3, 2.3 Hz, 1H), 5.49 (d, *J* = 2.2 Hz, 1H), 4.32 (app. sext, *J* = 7.5 Hz, 1H), 2.81 (s, 3H), 2.78–2.73 (m, 1H), 2.57 (td, *J* = 13.6, 5.0 Hz, 1H), 2.50–2.43 (m, 1H), 1.34 (d, *J* = 6.9 Hz, 3H), 1.26–1.11 (m, 1H); ^{13}C NMR (126 MHz, $CDCl_3$) δ 158.5, 144.4, 141.0, 140.1, 139.1, 137.8, 133.4, 133.3, 132.7, 132.2, 132.1, 128.3, 128.0, 127.4, 126.9, 126.0, 125.8, 125.2, 125.2, 125.1, 119.4, 118.8, 115.0, 108.7, 54.3, 34.7, 31.0, 29.7, 20.9; HRMS (ESI, m/z): calcd for $C_{29}H_{25}O$ $[M+H]^+$: 389.1899, found: 389.1898. Separation of the enantiomers was achieved by CSP-HPLC (Chiralcel OD-H, heptane:2-propanol = 98:2, flow rate = 0.5 mL/min, Rt: 17.35 min for (*Z*,*P*,*R*)-**3**, 21.50 min for (*Z*,*M*,*S*)-**3**.
(*E*)-**3**: m.p. 199–200 °C; ^{1}H NMR (500 MHz, $CDCl_3$) δ 7.95–7.84 (m, 3H), 7.71 (d, *J* = 8.3 Hz, 1H), 7.67 (d, *J* = 1.7 Hz, 1H), 7.54 (d, *J* = 7.4 Hz, 1H), 7.46 (d, *J* = 8.2 Hz, 1H), 7.36 (t, *J* = 7.4 Hz, 1H), 7.22 (t, *J* = 7.6 Hz, 2H), 7.02 (t, *J* = 7.4 Hz, 2H), 6.99 (dd, *J* = 8.3, 2.1 Hz, 1H), 6.48 (t, *J* = 7.7 Hz, 1H), 5.90 (d, *J* = 8.0 Hz, 1H), 4.29 (app. sext, *J* = 6.7 Hz, 1H), 3.96 (s, 3H), 2.80–2.70 (m, 1H), 2.58 (td, *J* = 13.3, 4.9 Hz, 1H), 2.51–2.35 (m, 1H), 1.28 (d, *J* = 6.9, 3H), 1.23–1.11 (m, 1H); ^{13}C NMR (126 MHz, $CDCl_3$) δ 159.3, 144.5, 139.8, 139.5, 139.5, 137.7, 134.2, 133.5, 133.4, 132.2, 132.0, 128.6, 128.2, 126.8, 126.7, 125.7, 125.4, 125.0, 124.9, 124.5, 120.1, 118.0, 112.2, 112.2, 55.7, 34.6, 30.9, 29.6, 20.7. HRMS (ESI, m/z): calcd for $C_{29}H_{25}O$ $[M+H]^+$: 389.1899, found: 389.1898. Separation of the enantiomers was achieved by CSP-HPLC (Chiralcel OD-H, heptane:2-propanol = 99:1, flow rate = 0.5 mL/min, Rt: 13.70 min for (*E*,*M*,*S*)-**3**, 25.50 min for (*E*,*P*,*R*)-**3**.

2.5.3 Irradiation experiments

Characterization and monitoring by UV-vis absorption and CD spectroscopy

Irradiation was performed using a Spectroline ENB-280C/FE lamp (for compounds (*Z*) & (*E*)-**1** and (*Z*) & (*E*)-**3** 312 nm was used, for compounds (*Z*) & (*E*)-**2** and (*Z*) & (*E*)-**4** 365 nm was used) or a Thorlabs INC OSL 1-EC fibre illuminator in combination with a cut-off filter (for compounds (*Z*) & (*E*)-**1** and (*Z*) & (*E*)-**3** 420 nm was used, for compounds (*Z*) & (*E*)-**2** and (*Z*) & (*E*)-**4** 450 nm was used). Solutions of enantiopure stable forms (heptane, $1.0 \cdot 10^{-5}$ M) were transferred in a quartz cuvette with magnetic stirrer and degassed with argon under stirring. The samples were irradiated under stirring over multiple cycles (2 min at 312/365 nm, 15–20 min at 420/450 nm) by placing the cuvette at a distance of 3 cm from the center of the lamp. To ensure the PSS was reached, several spectra were recorded at set intervals until no further changes were observed. Multiple UV-vis absorption spectra were recorded at set intervals during each cycle to follow both irradiation processes stepwise. CD spectra were recorded of starting solutions and after reaching the PSS mixtures at 312 or 365 nm as observed by UV-vis absorption.

Identification of (*Z*) and (*E*)-isomers of stable and metastable forms by ^{1}H NMR spectroscopy

The configuration of the (*Z*) and (*E*)-isomers of both the stable and metastable forms could be easily assigned by the difference in chemical shift of the absorption corresponding to the methoxy-substituent and protons in position 1 and 8 on the fluorenyl half in the ^{1}H NMR spectra. For example, in both stable-(*Z*)-**1** and metastable-(*Z*)-**1**, the chemical shift of the absorption corresponding to the methoxy-substituent is located in the range 3.50–3.40 ppm, while the proton in position 1 of the fluorenyl half (ortho to the methoxy-substituent) is located in the range 5.90–5.80 ppm. Similarly, in both stable-(*E*)-**1** and metastable-(*E*)-**1**, the chemical shift of the absorption corresponding to the methoxy-substituent is located in the range 3.95–3.90 ppm, while the proton in position 8 of the fluorenyl half is located in the range 6.25–6.15 ppm. These uncommon chemical shifts are caused by the atypical magnetic environment experienced by the aforementioned protons in each isomer when placed close to the aromatic part of the upper half. The chemical shifts differ of more than 0.5 ppm from their respective expected values, thus making the assignment of the isomers feasible. Similar analysis was performed for the other compounds described in this work (*vide supra*).

General procedure for irradiation experiments, characterization of metastable isomers and determination of the composition of the photostationary state by ^{1}H NMR spectroscopy

Stable isomers of **1**-**4** (~3 mg) were dissolved in $CDCl_3$ (0.6 mL). This sample was placed in an NMR tube and irradiated (312 or 365 nm) at a distance of 3 cm from the center of the lamp. ^{1}H NMR spectra of the sample were taken before, during and after irradiation at rt. No further changes were observed after 6 h of irradiation. For ^{1}H NMR spectra absorptions list of stable isomers, see characterization in the Synthetic procedures section. The relative integration of the absorptions peaks from the two isomers revealed PSS ratios of stable:metastable isomers at 312 or 365 nm) in $CDCl_3$ reported as follows.

metastable-(*E*)-**1**: ^{1}H NMR (500 MHz, $CDCl_3$) δ 7.62 (d, *J* = 8.3 Hz, 1H), 7.54–7.48 (m, 2H), 7.13–7.06 (m, 2H), 6.91 (dd, *J* = 8.3, 2.2 Hz, 1H), 6.80 (d, *J* = 7.6 Hz, 1H), 6.76 (t, *J* = 7.6 Hz, 1H), 6.17 (d, *J* = 7.9 Hz, 1H), 4.33–4.27 (m, 1H), 3.92 (s, 3H), 2.82–2.72 (m, 2H), 1.92 (s, 3H), 1.62 (d, *J* = 6.3 Hz, 3H). PSS ratio (312 nm) of stable-(*Z*)-**1** : metastable-(*E*)-**1** = 16:84.

metastable-(*Z*)-**1**: ^{1}H NMR (500 MHz, $CDCl_3$) 7.88 (d, *J* = 7.6 Hz, 1H), 7.60 (dd, *J* = 7.5, 1.3 Hz, 1H), 7.47 (d, *J* = 8.3 Hz, 1H), 7.32–7.22 (m, 2H), 7.07 (d, *J* = 7.6 Hz, 1H), 6.85 (d, *J* = 7.6 Hz, 1H), 6.72 (dd, *J* = 8.3, 2.4 Hz, 1H), 5.81 (d, *J* = 2.4 Hz, 1H), 4.36–4.30 (m, 1H), 3.43 (s, 3H), 2.78 (qd, *J* = 12.5, 3.0 Hz, 2H), 2.42 (s, 3H), 1.98 (s, 3H), 1.60 (d, *J* = 6.3 Hz, 3H). The relative integration of the absorptions peaks from the two isomers revealed a PSS ratio (312 nm) in $CDCl_3$ of stable-(*E*)-**1** : metastable-(*Z*)-**1** = 3:97.

metastable-(*E*)-**2**: ^{1}H NMR (500 MHz, $CDCl_3$) δ 7.73 (d, *J* = 8.5 Hz, 1H), 7.71–7.66 (m, 3H), 7.63 (d, *J* = 8.3 Hz, 1H), 7.56 (d, *J* = 8.4 Hz, 1H), 7.41 (dt, *J* = 7.5, 1.0 Hz, 1H), 7.19 (ddd, *J* = 8.0, 6.8, 1.2 Hz, 1H), 6.99 (ddd, *J* = 8.4, 6.8, 1.5 Hz, 1H), 6.95 (dd, *J* = 8.4, 2.3 Hz, 1H), 6.89 (td, *J* = 7.5, 1.1 Hz, 1H), 6.37 (ddd,

J = 8.3, 7.3, 1.2 Hz, 1H), 5.61 (d, *J* = 8.0 Hz, 1H), 4.63–4.55 (m, 1H), 3.95 (s, 3H), 2.96–2.82 (m, 2H), 1.69 (dd, *J* = 6.4, 0.9 Hz, 3H). PSS ratio (312 nm) of stable-(*Z*)-**2** : metastable-(*E*)-**2** = 14:86.

metastable-(*Z*)-**2**: ^{1}H NMR (500 MHz, $CDCl_3$) δ 8.05 (d, *J* = 7.5 Hz, 1H), 7.77 (d, *J* = 8.7 Hz, 1H), 7.72–7.67 (m, 2H), 7.63–7.59 (m, 1H), 7.58 (d, *J* = 8.5 Hz, 1H), 7.37 (d, *J* = 8.3 Hz, 1H), 7.35–7.28 (m, 2H), 7.23 (t, *J* = 7.5 Hz, 1H), 7.04 (t, *J* = 7.8 Hz, 1H), 6.51 (dd, *J* = 8.3, 2.3 Hz, 1H), 5.24 (d, *J* = 2.3 Hz, 1H), 4.68–4.60 (m, 1H), 3.02 (s, 3H), 2.95–2.83 (m, 2H), 1.67 (d, *J* = 6.3 Hz, 3H). PSS ratio (312 nm) of stable-(*E*)-**2** : metastable-(*Z*)-**2** = 5:95.

metastable-(*E*)-**3**: ^{1}H NMR (500 MHz, $CDCl_3$) δ 7.80 (d, *J* = 8.3 Hz, 1H), 7.78 (dd, *J* = 8.7, 1.1 Hz, 1H), 7.73 (dd, *J* = 8.0, 1.4 Hz, 1H), 7.68 (d, *J* = 2.2 Hz, 1H), 7.66 (d, *J* = 8.3 Hz, 1H), 7.50–7.46 (m, 1H), 7.42 (d, *J* = 8.2 Hz, 1H), 7.24–7.19 (m, 1H), 7.00 (ddd, *J* = 8.5, 6.8, 1.4 Hz, 1H), 6.97–6.91 (m, 2H), 6.40 (ddd, *J* = 8.2, 7.3, 1.2 Hz, 1H), 5.92 (d, *J* = 7.8 Hz, 1H), 4.10 (app. p, *J* = 6.7 Hz, 1H), 3.95 (s, 3H), 3.07–2.98 (m, 1H), 2.79–2.72 (m, 1H), 1.96–1.89 (m, 1H), 1.56 (d, *J* = 6.7 Hz, 3H). PSS ratio (312 nm) of stable-(*Z*)-**3** : metastable-(*E*)-**3** = 12:88.

metastable-(*Z*)-**3**: ^{1}H NMR (500 MHz, $CDCl_3$) δ 8.07 (d, *J* = 8.8 Hz, 1H), 7.85 (d, *J* = 8.8 Hz, 1H), 7.78 (d, *J* = 8.2 Hz, 1H), 7.74 (d, *J* = 8.2 Hz, 1H), 7.66–7.63 (m, 1H), 7.43 (dd, *J* = 8.3, 1.6 Hz, 2H), 7.31 (tt, *J* = 7.4, 5.9 Hz, 2H), 7.25 (d, *J* = 8.1 Hz, 1H), 7.08–7.01 (m, 1H), 6.55 (dd, *J* = 8.3, 2.4 Hz, 1H), 5.52 (d, *J* = 2.3 Hz, 1H), 4.15 (app. p, *J* = 6.5 Hz, 1H), 3.10–3.00 (m, 1H), 2.93 (s, 3H), 2.76 (dt, *J* = 15.1, 3.1 Hz, 1H), 1.97–1.90 (m, 1H), 1.55 (d, *J* = 6.7 Hz, 3H). PSS ratio (312 nm) of stable-(*E*)-**3** : metastable-(*Z*)-**3** = 5:95.

Collected ^{1}H NMR spectra of stable isomers and PSS mixtures of compounds 1-3

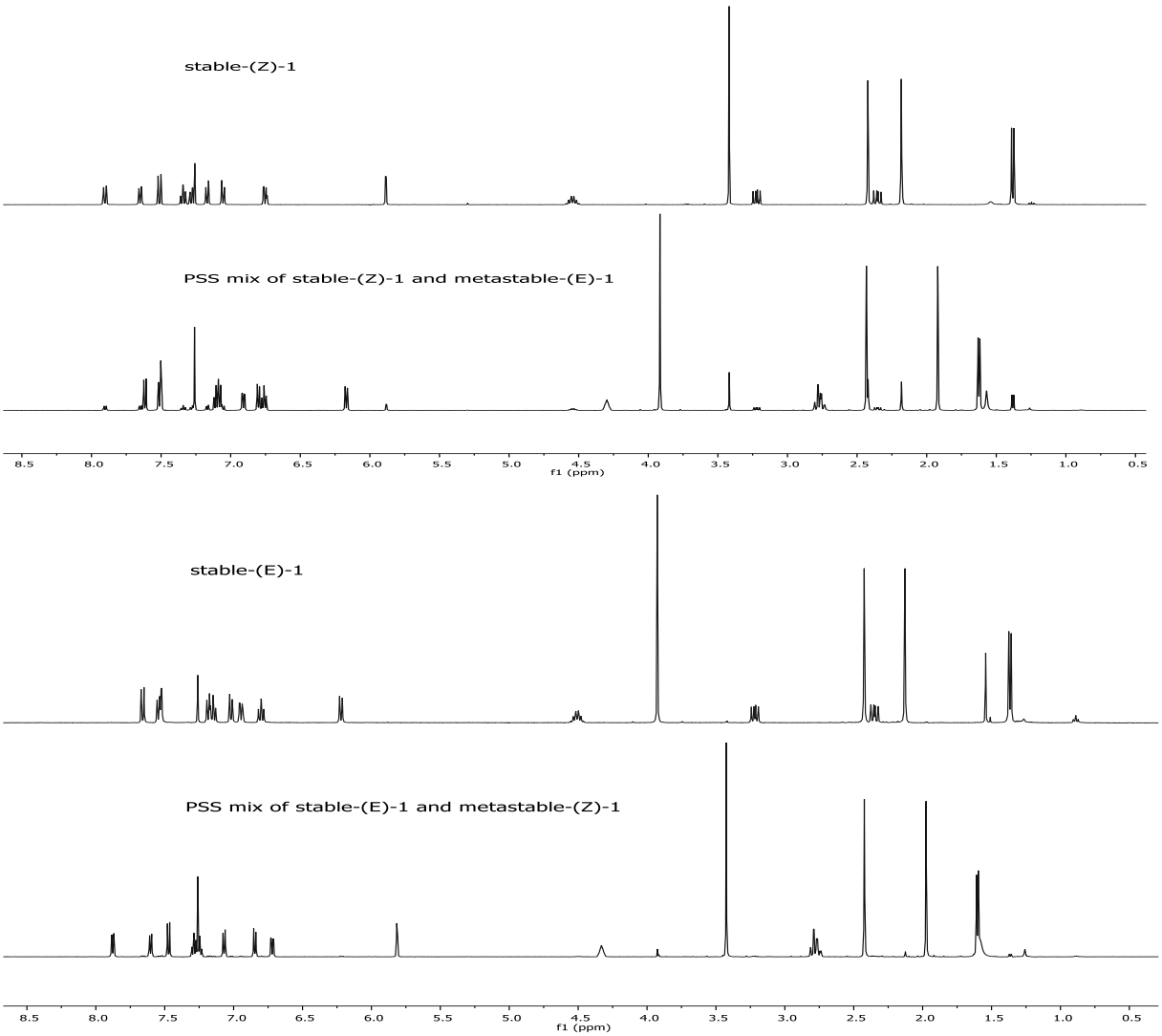

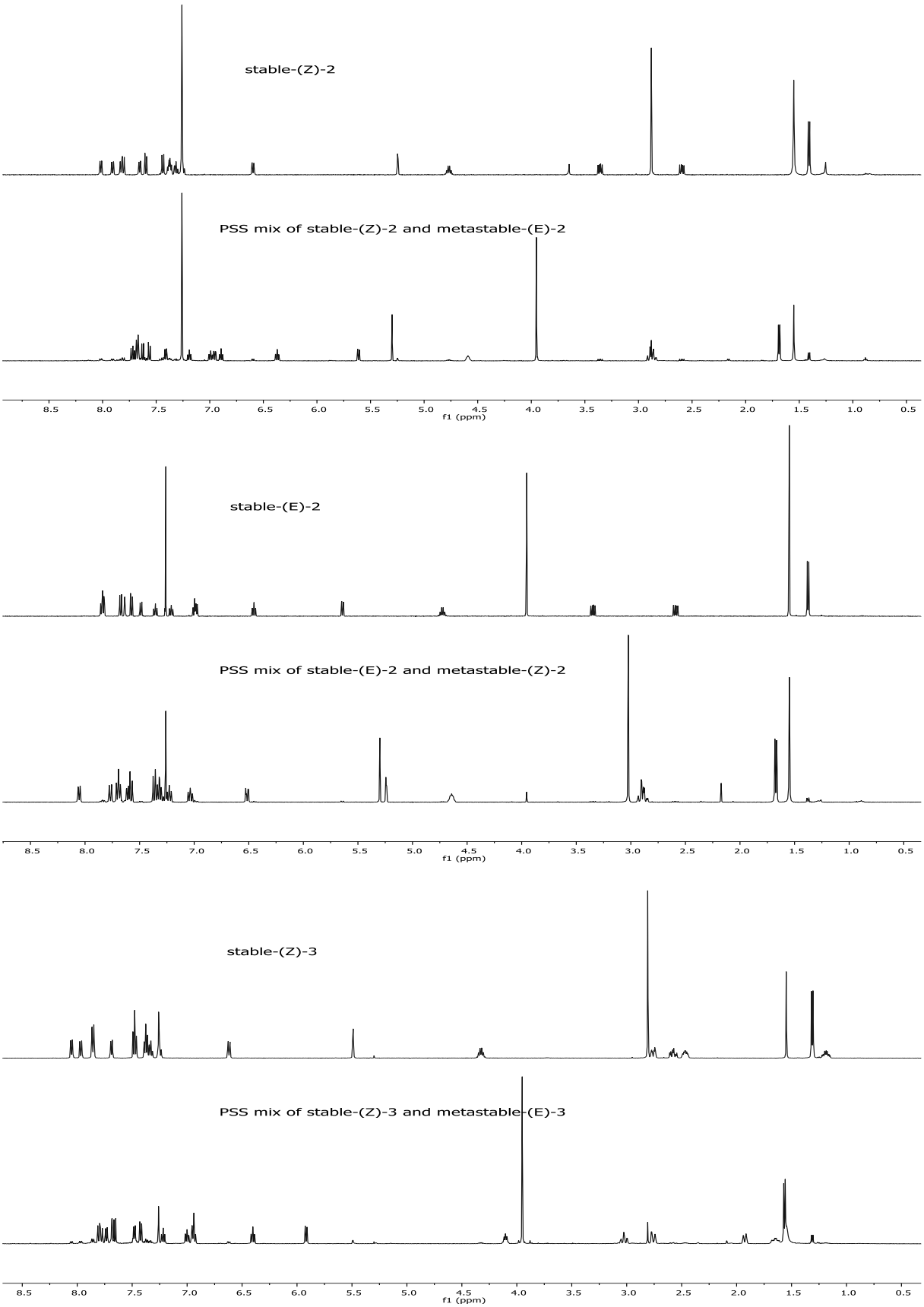
stable-(Z)-2
PSS mix of stable-(Z)-2 and metastable-(E)-2
8.5 8.0 7.5 7.0 6.5 6.0 5.5 5.0 4.5 4.0 3.5 3.0 2.5 2.0 1.5 1.0 0.5
f1 (ppm)
stable-(E)-2
PSS mix of stable-(E)-2 and metastable-(Z)-2
8.5 8.0 7.5 7.0 6.5 6.0 5.5 5.0 4.5 4.0 3.5 3.0 2.5 2.0 1.5 1.0 0.5
f1 (ppm)
stable-(Z)-3
PSS mix of stable-(Z)-3 and metastable-(E)-3
8.5 8.0 7.5 7.0 6.5 6.0 5.5 5.0 4.5 4.0 3.5 3.0 2.5 2.0 1.5 1.0 0.5
f1 (ppm)

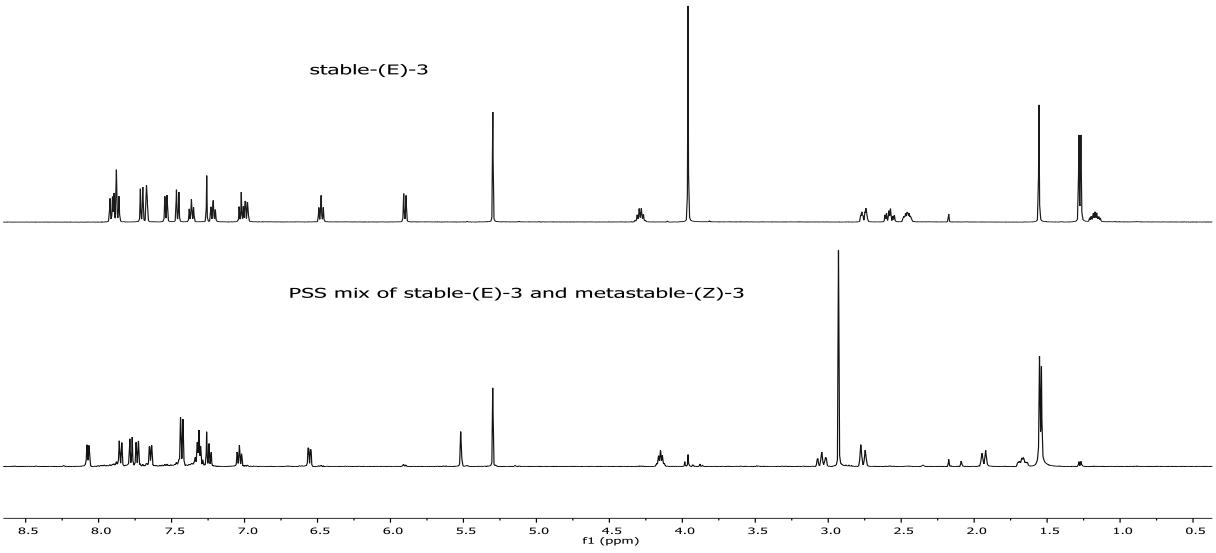

2.5.4 Kinetic experiments via thermal decay

(*Z*) & (*E*)-1. A flame-died Schlenk tube equipped with stirring bar and filled with argon was loaded with hexanol (99% purity grade, 1.5 mL), then a solution of optically pure stable-(*Z*)-**1** or stable-(*E*)-**1** in hexanol (0.5 mL, ~10^{-5} M) previously irradiated with UV light (312 nm) to reach the photostationary state was injected in the tube. The solution obtained was freeze-thawed 3 times and the tube was filled with argon. The tube was placed in a preheated oil bath at a fixed temperature (ranging from 131 ºC to 152 ºC) and stirred for ~ 6 h (see corresponding Figure 2.3 or Figure 2.S6 for further details). At set time intervals (ranging from 10 min to 300 min) an aliquot (~0.1 mL) was withdrawn and cooled in a HPLC vial containing heptane (~0.2 mL). The temperature of the oil baths during the kinetics experiments were measured with a Pt1000 RTD Temperature Sensor. Analysis by chiral HPLC (the same methods used for the isolation of the pure enantiomers were applied to the analysis), setting the wavelength of the analysis at the specific isosbestic point (λ = 344 nm), afforded the data for monitoring the decay of metastable-(*E*)-**1** or metastable-(*Z*)-**1** and the formation of the stable-(*Z*)-**1** and stable-(*E*)-**1**.

(*Z*) & (*E*)-2. A flame-died Schlenk tube equipped with stirring bar and filled with argon was charged with dodecane (99% purity grade, 1.5 mL), then a solution of optically pure stable-(*Z*)-**2** or stable-(*E*)-**2** in dodecane (0.5 mL, ~10^{-5} M) was injected in the tube. The solution obtained was bubbled with argon for 5 min and irradiated with UV light (365 nm) to reach photostationary state after 30 min. Then the tube was placed in a preheated oil bath at a fixed temperature (ranging from 112 ºC to 140 ºC) and stirred for ~5 h (see corresponding Figure 2.3 or Figure 2.S6 for further details). At a set of time intervals (ranging from 10 min to 300 min) an aliquot (~0.1 mL) was withdrawn and quenched in a HPLC-vial containing heptane (~0.2 mL). The temperature of oil baths during the kinetics experiments were measured with a Pt1000 RTD Temperature Sensor. Analysis by chiral HPLC (the same programs used for the isolation of the pure enantiomers were applied to the analysis), setting the wavelength of the analysis at the specific isosbestic point (λ = 366 nm), afforded the data for monitoring the decay of metastable-(*E*)-**1** or metastable-(*Z*)-**2** and the formation of the stable-(*Z*)-**1** and stable-(*E*)-**1**.

(*Z*) & (*E*)-3. A UV-vis quartz cuvette with screw cap was filled with a solution of optically pure stable-(*Z*)-**3** or stable-(*E*)-**3** in dodecane (~10^{-5} M) previously bubbled with argon and irradiated with UV light (312 nm) to reach photostationary state. The cuvette was transferred into a CD spectrometer equipped with a Peltier temperature control cell preheated at a fixed temperature (ranging from 95 ºC to 107 ºC) and heated over 24 h (see corresponding Figure 2.3 or Figure 2.S6 for further details). The decay process was followed

via time course experiment by monitoring the change in CD signal at λ = 381 nm (wavelength of maximal CD signal difference) over time. Analysis by chiral HPLC (the same programs used for the isolation of the pure enantiomers were applied to the analysis) of the final solutions after completion of decay process of metastable-(*E*)-**3** afforded the final ratio of stable-(*Z*)-**3** and stable-(*E*)-**3**.

(*Z*)-4. A UV-vis quartz cuvette with screw cap was filled with a solution of optically pure stable-(*Z*)-**4** in dodecane (~10^{-5} M) bubbled with argon and irradiated with UV light (312 nm) to reach photostationary state. The cuvette was transferred into a CD spectrometer equipped with a Peltier temperature control cell preheated at a fixed temperature (ranging from 84 ºC to 105 ºC) and heated over 24 h (see corresponding Figure 2.3 for further details). The decay process was followed by a time course experiment, monitoring the change in CD signal at λ = 395 nm over time. Analysis by chiral HPLC (the same program used for the isolation of the pure enantiomer was applied to the analysis) of the final solutions after completion of decay process of metastable-(*E*)-**4** afforded the final ratio of stable-(*Z*)-**4** and stable-(*E*)-**4**.

2.5.5 Collected PSS ratios and TEZI/THI ratios of compounds 1-4

The TEZI/THI ratios of stable products after thermal decay of each metastable form were calculated at the corresponding temperature at which the half-life is 1 h (T at $t_{1/2}$ = 1 h) from the determined thermodynamic parameters (see main text, Table 1 for (*Z*)-**1**–**4** and Experimental section, Table 2.4 for (*E*)-**1**–**3**):

Compound (*Z*)-**1**
PSS (312 nm): stable-(*Z*)-**1** : metastable-(*E*)-**1** = 5:95
PSS (420 nm): stable-(*Z*)-**1** : metastable-(*E*)-**1** = 64:36
TEZI/THI-ratio at T at $t_{1/2}$ = 1 h (138.2 °C): stable-(*Z*)-**1** : stable-(*E*)-**1** = 93:7

Compound (*E*)-**1**
PSS (312 nm): stable-(*E*)-**1** : metastable-(*Z*)-**1** = 3:97
PSS (420 nm): stable-(*E*)-**1** : metastable-(*Z*)-**1** = 64:36
TEZI/THI-ratio at T at $t_{1/2}$ = 1 h (144.6 °C): stable-(*Z*)-**1** : stable-(*E*)-**1** = 95:5

Compound (*Z*)-**2**
PSS (365 nm): stable-(*Z*)-**2** : metastable-(*E*)-**2** = 4:96
PSS (450 nm): stable-(*Z*)-**2** : metastable-(*E*)-**2** = 82:18
TEZI/THI-ratio at T at $t_{1/2}$ = 1 h (129.3 °C): stable-(*Z*)-**1** : stable-(*E*)-**1** = 96:4

Compound (*E*)-**2**
PSS (312 nm): stable-(*E*)-**2** : metastable-(*Z*)-**2** = 20:80
PSS (420 nm): stable-(*E*)-**2** : metastable-(*Z*)-**2** = 94:6
TEZI/THI-ratio at T at $t_{1/2}$ = 1 h (126.7 °C): stable-(*Z*)-**1** : stable-(*E*)-**1** = 97:3

Compound (*Z*)-**3**
PSS (312 nm): stable-(*Z*)-**3** : metastable-(*E*)-**3** = 3:97
PSS (420 nm): stable-(*Z*)-**3** : metastable-(*E*)-**3** = 93:7
TEZI/THI-ratio at T at $t_{1/2}$ = 1 h (116.0 °C): stable-(*Z*)-**1** : stable-(*E*)-**1** = 70:30

Compound (*E*)-**3**
PSS (365 nm): stable-(*E*)-**3** : metastable-(*Z*)-**3** = 2:98
PSS (450 nm): stable-(*E*)-**3** : metastable-(*Z*)-**3** = 75:25

TEZI/THI-ratio at T at $t_{1/2}$ = 1 h (122.3 °C): stable-(*Z*)-**1** : stable-(*E*)-**1** = 81:19

Compound (*Z*)-**4**
PSS (312 nm): stable-(*Z*)-**4** : metastable-(*E*)-**4** = 1:99
PSS (420 nm): stable-(*Z*)-**4** : metastable-(*E*)-**4** = 70:30
TEZI/THI-ratio at T at $t_{1/2}$ = 1 h (99.1 °C): stable-(*Z*)-**4** : stable-(*E*)-**4** = 68:32

2.6 References

(1) H.-J. Schneider, Ed., Chemoresponsive Materials, Royal Society of Chemistry, Cambridge, **2015**.
(2) J. Zhang, Q. Zou, H. Tian, *Adv. Mater.* **2013**, *25*, 378–399.
(3) H. Dong, H. Zhu, Q. Meng, X. Gong, W. Hu, *Chem. Soc. Rev.* **2012**, *41*, 1754–1808.
(4) A. Coskun, M. Banaszak, R. D. Astumian, J. F. Stoddart, B. A. Grzybowski, *Chem. Soc. Rev.* **2012**, *41*, 19–30.
(5) B. L. Feringa, W. R. Browne, *Molecular Switches Vol. I, II*, Wiley-VCH Verlag GmbH & Co. KGaA, Weinheim, Germany, **2011**.
(6) W. R. Browne, B. L. Feringa, *Nat. Nanotechnol.* **2006**, *1*, 25–35.
(7) M. Schliwa, *Molecular Motors*, Wiley-VCH Verlag GmbH, **2006**.
(8) M. Schliwa, G. Woehlke, *Nature* **2003**, *422*, 759–765.
(9) E. R. Kay, D. A. Leigh, F. Zerbetto, *Angew. Chem. Int. Ed.* **2007**, *46*, 72–191.
(10) M. von Delius, D. A. Leigh, *Chem. Soc. Rev.* **2011**, *40*, 3656–3676.
(11) F. D. Jochum, P. Theato, *Chem. Soc. Rev.* **2013**, *42*, 7468–7483.
(12) Q. Yan, Z. Luo, K. Cai, Y. Ma, D. Zhao, *Chem. Soc. Rev.* **2014**, *43*, 4199–4221.
(13) M. Schwartz, *Smart Materials*, CRC Press, **2008**.
(14) M. W. Urban, Ed., *Handbook of Stimuli-Responsive Materials*, Wiley-VCH Verlag GmbH & Co. KGaA, Weinheim, Germany, **2011**.
(15) M. Shahinpoor, H.-J. Schneider, Eds., *Intelligent Materials*, Royal Society of Chemistry, Cambridge, **2007**.
(16) M. A. C. Stuart, W. T. S. Huck, J. Genzer, M. Müller, C. Ober, M. Stamm, G. B. Sukhorukov, I. Szleifer, V. V Tsukruk, M. Urban, et al., *Nat. Mater.* **2010**, *9*, 101–113.
(17) J. Thévenot, H. Oliveira, O. Sandre, S. Lecommandoux, *Chem. Soc. Rev.* **2013**, *42*, 7099–7116.
(18) Y. Shirota, H. Kageyama, *Chem. Rev.* **2007**, *107*, 953–1010.
(19) N. Koch, Ed. , *Supramolecular Materials for Opto-Electronics*, Royal Society Of Chemistry, Cambridge, **2014**.
(20) C. J. Bruns, J. F. Stoddart, *Acc. Chem. Res.* **2014**, *47*, 2186–2199.
(21) G. Du, E. Moulin, N. Jouault, E. Buhler, N. Giuseppone, *Angew. Chem. Int. Ed.* **2012**, *51*, 12504–12508.
(22) A. Coskun, J. M. Spruell, G. Barin, W. R. Dichtel, A. H. Flood, Y. Y. Botros, J. F. Stoddart, *Chem. Soc. Rev.* **2012**, *41*, 4827–4859.
(23) T. Kudernac, N. Ruangsupapichat, M. Parschau, B. Maciá, N. Katsonis, S. R. Harutyunyan, K.-H. Ernst, B. L. Feringa, *Nature* **2011**, *479*, 208–211.
(24) J. Wang, B. L. Feringa, *Science* **2011**, *331*, 1429–1432.
(25) S. J. Wezenberg, M. Vlatković, J. C. M. Kistemaker, B. L. Feringa, *J. Am. Chem. Soc.* **2014**, *136*, 16784–16787.
(26) W. M. Horspool, F. Lenci, *CRC Handbook of Organic Photochemistry and Photobiology, Vol. 1 & 2*, CRC Press, Boca Raton, USA, **2003**.
(27) G. S. Kottas, L. I. Clarke, D. Horinek, J. Michl, *Chem. Rev.* **2005**, *105*, 1281–1376.
(28) B. L. Feringa, *J. Org. Chem.* **2007**, *72*, 6635–6652.
(29) N. Koumura, R. W. Zijlstra, R. A. van Delden, N. Harada, B. L. Feringa, *Nature* **1999**, *401*, 152–155.
(30) N. Koumura, E. M7. Geertsema, M. B. van Gelder, A. Meetsma, B. L. Feringa, *J. Am. Chem. Soc.* **2002**, *124*, 5037–5051.
(31) J. C. M. Kistemaker, P. Štacko, J. Visser, B. L. Feringa, *Nat. Chem.* **2015**, *7*, 890–896.

(32) E. M. Geertsema, S. J. van der Molen, M. Martens, B. L. Feringa, *Proc. Natl. Acad. Sci. U. S. A.* **2009**, *106*, 16919–16924.
(33) R. A. van Delden, M. K. J. ter Wiel, H. de Jong, A. Meetsma, B. L. Feringa, *Org. Biomol. Chem.* **2004**, *2*, 1531–1541.
(34) J. Vicario, A. Meetsma, B. L. Feringa, *Chem. Commun.* **2005**, 5910–5912.
(35) D. Pijper, R. A. van Delden, A. Meetsma, B. L. Feringa, *J. Am. Chem. Soc.* **2005**, *127*, 17612–17613.
(36) J. Vicario, M. Walko, A. Meetsma, B. L. Feringa, *J. Am. Chem. Soc.* **2006**, *128*, 5127–5135.
(37) M. M. Pollard, M. Lubomska, P. Rudolf, B. L. Feringa, *Angew. Chem. Int. Ed.* **2007**, *46*, 1278–1280.
(38) M. Klok, N. Boyle, M. T. Pryce, A. Meetsma, W. R. Browne, B. L. Feringa, *J. Am. Chem. Soc.* **2008**, *130*, 10484–10485.
(39) A. Cnossen, D. Pijper, T. Kudernac, M. M. Pollard, N. Katsonis, B. L. Feringa, *Chem. Eur. J.* **2009**, *15*, 2768–2772.
(40) T. C. Pijper, D. Pijper, M. M. Pollard, F. Dumur, S. G. Davey, A. Meetsma, B. L. Feringa, *J. Org. Chem.* **2010**, *75*, 825–838.
(41) A. A. Kulago, E. M. Mes, M. Klok, A. Meetsma, A. M. Brouwer, B. L. Feringa, *J. Org. Chem.* **2010**, *75*, 666–679.
(42) L. F. Tietze, M. A. Düfert, T. Hungerland, K. Oum, T. Lenzer, *Chemistry* **2011**, *17*, 8452–8461.
(43) L. Greb, J.-M. Lehn, *J. Am. Chem. Soc.* **2014**, *136*, 13114–13117.
(44) J. Bauer, L. Hou, J. C. M. Kistemaker, B. L. Feringa, *J. Org. Chem.* **2014**, *79*, 4446–4455.
(45) M. K. J. ter Wiel, R. A. van Delden, A. Meetsma, B. L. Feringa, *J. Am. Chem. Soc.* **2005**, *127*, 14208–14222.
(46) R. Göstl, A. Senf, S. Hecht, *Chem. Soc. Rev.* **2014**, *43*, 1982–1996.
(47) V. Blanco, D. A. Leigh, V. Marcos, *Chem. Soc. Rev.* **2015**, *44*, 5341–70.
(48) M. Klok, M. Walko, E. M. Geertsema, N. Ruangsupapichat, J. C. M. Kistemaker, A. Meetsma, B. L. Feringa, *Chemistry* **2008**, *14*, 11183–11193.
(49) G. B. Kistiakowsky, W. R. Smith, *J. Am. Chem. Soc.* **1934**, *56*, 638–642.
(50) A. V. Santoro, E. J. Barrett, H. W. Hoyer, *J. Am. Chem. Soc.* **1967**, *89*, 4545–4546.
(51) I. Agranat, M. Rabinovitz, A. Weitzen-Dagan, I. Gosnay, *J. Chem. Soc. Chem. Commun.* **1972**, 732–733.
(52) P. U. Biedermann, J. J. Stezowski, I. Agranat, *European J. Org. Chem.* **2001**, *2001*, 15–34.
(53) A. Kazaryan, J. C. M. Kistemaker, L. V Schäfer, W. R. Browne, B. L. Feringa, M. Filatov, *J. Phys. Chem. A* **2010**, *114*, 5058–5067.
(54) G. Pérez-Hernández, L. González, *Phys. Chem. Chem. Phys.* **2010**, *12*, 12279–12289.
(55) A. Cnossen, J. C. M. Kistemaker, T. Kojima, B. L. Feringa, *J. Org. Chem.* **2014**, *79*, 927–935.
(56) B. O. Roos, P. R. Taylor, P. E. M. Siegbahn, *Chem. Phys.* **1980**, *48*, 157–173.
(57) It is noted that multi-reference methods based on the density matrix renormalization group (DMRG) approach are capable of handling much larger active spaces. Unfortunately, however, this approach is unavailable in almost all QC software package**.**
(58) N. Ruangsupapichat, M. M. Pollard, S. R. Harutyunyan, B. L. Feringa, *Nat. Chem.* **2011**, *3*, 53–60.
(59) D. J. van Dijken, J. Chen, M. C. A. Stuart, L. Hou, B. L. Feringa, *J. Am. Chem. Soc.* **2016**, *138*, 660–669.
(60) N. Berova, P. L. Polavarapu, K. Nakanishi, R. W. Woody, Eds. , *Comprehensive Chiroptical Spectroscopy*, John Wiley & Sons, Inc., Hoboken, NJ, USA, **2012**.
(61) Forst, W. *Theory of Unimolecular Reactions*; Academic Press: New York, **2012**.
(62) The Lambert W function solves y=x.e^x for x as x=W(y), see ref. 32 for further details.
(63) Despite considerable overlap in the UV, the PSS towards MS is nearly quantatative while the reverse PSS towards stable is not, indicating that stable to MS quantum yields are much higher than MS to stable quantum yields. This has also been observed by Cnossen et al. (see ref. 55) for a series of second generation molecular motors.
(64) Koumura, N.; Geertsema, E. M.; van Gelder, M. B.; Meetsma, A.; Feringa, B. L. *J. Am. Chem. Soc.* **2002**, *124*, 5037–5051.
(65) Pijper, T. C.; Pijper, D.; Pollard, M. M.; Dumur, F.; Davey, S. G.; Meetsma, A.; Feringa, B. L. *J. Org. Chem.* **2010**, *75*, 825–838.
(66) Harada, N.; Koumura, N.; Feringa, B. L. *J. Am. Chem. Soc.* **1997**, *119*, 7256–7264.